Atmos. Chem. Phys., 10, 11189–11208, 2010
www.atmos-chem-phys.net/10/11189/2010/
doi:10.5194/acp-10-11189-2010

Atmospheric Chemistry and Physics

Observations of ozone production in a dissipating tropical convective cell during TC4

G. A. Morris[1], **A. M. Thompson**[2], **K. E. Pickering**[3], **S. Chen**[2], **E. J. Bucsela**[4], **and P. A. Kucera**[5]

[1]Dept. of Physics and Astronomy, Valparaiso University, Valparaiso, IN, USA
[2]Dept. of Meteorology, Pennsylvania State University, University Park, PA, USA
[3]Atmospheric Chemistry and Dynamics Branch, Laboratory for Atmospheres, NASA Goddard Space Flight Center, Greenbelt, MD, USA
[4]SRI International, Menlo Park, CA, USA
[5]Research Applications Laboratory, NCAR, Boulder, CO, USA

Received: 10 July 2010 – Published in Atmos. Chem. Phys. Discuss.: 11 August 2010
Revised: 10 November 2010 – Accepted: 11 November 2010 – Published: 26 November 2010

Abstract. From 13 July–9 August 2007, 25 ozonesondes were launched from Las Tablas, Panama as part of the Tropical Composition, Cloud, and Climate Coupling (TC4) mission. On 5 August, a strong convective cell formed in the Gulf of Panama. World Wide Lightning Location Network (WWLLN) data indicated 563 flashes (09:00–17:00 UTC) in the Gulf. NO_2 data from the Ozone Monitoring Instrument (OMI) show enhancements, suggesting lightning production of NO_x. At 15:05 UTC, an ozonesonde ascended into the southern edge of the now dissipating convective cell as it moved west across the Azuero Peninsula. The balloon oscillated from 2.5–5.1 km five times (15:12–17:00 UTC), providing a unique examination of ozone (O_3) photochemistry on the edge of a convective cell. Ozone increased at a rate of ∼1.6–4.6 ppbv/hr between the first and last ascent, resulting cell wide in an increase of $\sim(2.1–2.5) \times 10^6$ moles of O_3. This estimate agrees to within a factor of two of our estimates of photochemical lightning O_3 production from the WWLLN flashes, from the radar-inferred lightning flash data, and from the OMI NO_2 data (∼1.2, ∼1.0, and $\sim1.7 \times 10^6$ moles, respectively), though all estimates have large uncertainties. Examination of DC-8 in situ and lidar O_3 data gathered around the Gulf that day suggests 70–97% of the O_3 change occurred in 2.5–5.1 km layer. A photochemical box model initialized with nearby TC4 aircraft trace gas data suggests these O_3 production rates are possible with our present understanding of photochemistry.

Correspondence to: G. A. Morris
(gary.morris@valpo.edu)

1 Introduction

Numerous studies in the latter half of the 20-th Century have examined the role of lightning in global and regional ozone (O_3) (e.g., Kroening and Ney, 1962; Orville, 1967; Griffing, 1977; Levine, et al., 1981; Pickering et al., 1990; Lelieveld and Crutzen, 1994; Lawrence et al., 2003; Doherty et al., 2005; Cooper et al., 2006; see also Table 1) and in particular, its photochemical production resulting from lightning-produced reactive nitrogen (NO_x) (Noxon, 1976; Chameides et al., 1977, 1979; Peyrous and Lepeyre, 1982). With refinements in regional and global models and lightning flash data from satellites and ground-based networks, the global lightning NO_x ($LtNO_x$) budget has been reliably set at 2–8 Tg N/year (Pickering et al., 2009; Schumann and Huntrieser, 2007; Lawrence et al., 1995). Photochemical reactions involving $LtNO_x$ lead to O_3 formation. Grewe (2007) estimates the global lightning contribution to tropospheric O_3 at >30%, with the fractional source greatest in the tropics.

Laboratory studies have suggested that direct production of O_3 occurs mainly during the pre-discharge period of storms (Peyrous and Lapeyre, 1982), and Franzblau (1991) found (1) little O_3 production except at very low energies, (2) large decreases in O_3 immediately after discharges, and (3) nearly full recovery to pre-discharge levels after ∼10 min (see his Fig. 1).

A number of field campaigns and modeling studies have attempted to identify the role of lightning in the formation and/or destruction of tropospheric ozone, and the role of convective activity in the redistribution of NO_x, O_3, and other trace species within the troposphere. The results from these

Table 1. Summary of previous studies of O_3 production.

Observation	Location	Instrument/Model	Citation
O_3 aloft = 2–3 × pre-storm surface O_3.	New Mexico	Ozonesonde	Schlanta and Moore (1972)
+300 ppbv of O_3 near 1 km in thunderstorm	Maryland	Aircraft	Clark and Griffing (1985)
Peak O_3 detected at 5 km, secondary peak at 10 km	Midwest USA	Aircraft (PRE-STORM project)	Dickerson et al. (1987)
The highest O_3 production potential found below 5 km following deep convection; dissipating cell 7–17 ppbv/day @ 1–6 km (their Fig. 14)	South Central USA	Aircraft (PRE-STORM) + 1-D photochemical model	Pickering et al. (1990)
Convection enhances O_3 <6.5 km at 5° N (their Fig. 1)	Global analysis	Global 3-D model	Lelieveld and Crutzen (1994)
7–8 ppbv/day of O_3 produced downwind of thunderstorms at 8–12 km	Brazil	DC-8, Ozonesondes + GCE model	Pickering et al. (1996) and Thompson et al. (1997)
Most $LtNO_x$ is produced below 5 km by CG flashes	Global analysis	International Satellite Cloud Climatology Project	Price et al. (1997)
+38 ppbv O_3 in convective cloud	France	DOAS + GOMETRAN model	Winterrath et al. (1999)
+12% of tropospheric O_3 due to convection	Global analysis	MATCH-MPIC model	Lawrence et al. (2003)
10–20% of tropospheric O_3 from lightning at 2–6 km; 20–30% at 6–12 km @ ∼10° N.	Global analysis	MOZART model	Zhang et al. (2003)
+2 ppbv of O_3 during storm, +10 ppbv/24 h in UT (5–10 km)	USA high plains	STERAO-A + CSCTM and GCE models	DeCaria et al. (2005)
In the tropics, convection reduces O_3 by 1–3 ppbv < 1.5 km and increases O_3 by 1–5 ppbv from 1.5–5.5 km (Fig. 3), but globally, convection reduces tropospheric O_3 by 13%.	Global analysis	STOCHEM-HadAM3	Doherty et al. (2005)
80% of O_3 above background due to $LtNO_x$; $P(O_3)$ = +3–4 ppbv/day; 16–24 ppbv O_3 in UT	Southeast USA and Texas	Ozonesondes (IONS-04) + Flexpart model	Cooper et al. (2006)
6–8 ppbv lower O_3 in convective cell	Tropical Pacific	Aircraft (PEM-Tropics B)	Ridley et al. (2006)
$LtNO_x$ leads to +25–30 ppbv of O_3 @10 km	Southeast USA	Ozonesondes (IONS-06) + Flexpart model	Cooper et al. (2007)
+10–15 DU of O_3 downwind of convection and biomass burning	Tropical Atlantic	SCIAMACHY	Martin et al. (2007)

studies vary widely, with some suggesting strong enhancements of O_3 (e.g., Schlanta and Moore, 1972; Dickerson et al., 1987) and others suggesting no such enhancements and potential losses of O_3 (e.g., Ridley et al., 2006; Ott et al., 2007; Salzmann et al., 2008). Results from these previous studies are summarized in Table 1.

The TC4 campaign (Toon et al., 2010) was an excellent vehicle to further investigate wave activity, lightning, and O_3 responses in a highly-convective environment, closer to the Intertropical Convergence Zone than the August–September Intercontinental Transport Experiment (INTEX)-B Ozonesonde Network Study (IONS-06) soundings (e.g.,

Table 1. Continued.

Observation	Location	Instrument/Model	Citation
9 ppbv lower O_3 during 3 h of storm, but+5 ppbv/day downwind @ 5.5 km	Europe	European Lightning Nitrogen Oxides Project + GCE model	Ott et al. (2007)
+7 DU of O_3; 80% O_3 from storms @ 2.5–10 km	Tropical Atlantic	Ozonesondes + LIS + RegCM3 model	Jenkins et al. (2008)
Direct production of 0.2–2.0×10^{27} molecules O_3 per flash; mechanism produces ∼21% as much O_3 as photochemistry	New Mexico	Ozonesonde	Minschwaner et al. (2008)
10% of tropospheric O_3 from lightning	North America	Ozonesonde (IONS-04) + CTM model	Pfister et al. (2008)
Maximum O_3 loss at 5 km during storm	Western Pacific	CSRMC model for TOGA COARE/CEPEX	Salzmann et al. (2008)

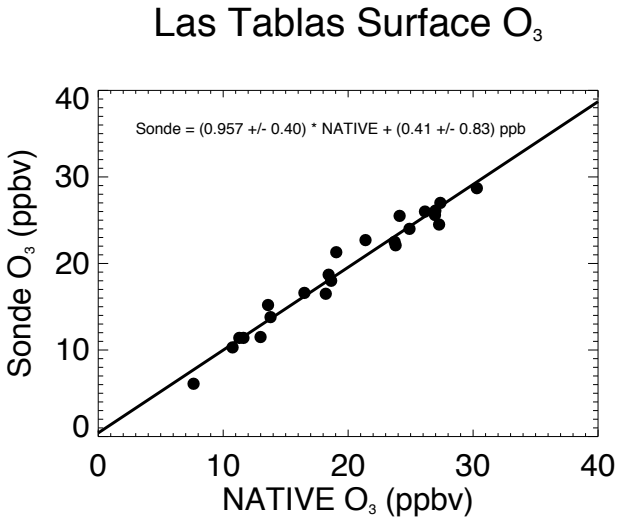

Fig. 1. A comparison between the ozonesonde readings and NATIVE surface O_3 measurements at the time of launch. Agreement is good to within ∼5% during the TC-4 campaign.

Thompson et al., 2008). The concentration of new satellite products and aircraft instrumentation focused on convection permits us to quantify lightning, to relate flashes to improved representations in models, and to link the latter to validation of NO_2 from the Ozone Measuring Instrument (OMI) aboard the NASA Aura satellite (e.g., Bucsela et al., 2010).

In addition to O_3 measurements on the three TC4 aircraft, the Southern Hemisphere Additional OZonedondes (SHADOZ) (Thompson et al., 2003) Costa Rican station (Heredia, 10° N, 84° W) and the TC4 site at Las Tablas, Panama (7.75° N, 80.25° W; see also Thompson et al., 2010) provided O_3 profiles. Virtually all the Costa Rican and Panama soundings contained free-tropospheric (FT) and lower-stratospheric wave signatures, with an incidence in the tropical tropopause layer (TTL) of >40% (see Fig. 2a in Thompson et al., 2010). Case studies of O_3 within segments affected by gravity waves demonstrated a clear link to convective activity.

The 25 Panama sondes, in a region with a high convective frequency during TC4 (Toon et al., 2010), displayed prominent wave activity associated with convection near the beginning of the mission (13–22 July 2007) and after 2 August 2007, when the TC4 aircraft coordinated sampling south of Costa Rica, in the vicinity of the Panama Bight, and as far south as the Galapagos. On 5 August, a day when all three TC4 aircraft flew over the Panama Bight, the ozonesonde launched from Las Tablas was caught in a convective system that kept it oscillating between 2.5–5.1 km for nearly two hours before it resumed normal ascent. Though many previous studies provided profiles before and after convection, this ozonesonde data set is unique in providing insights into changing O_3 concentrations inside a dissipating tropical convective cell. Ozone increased throughout the oscillatory period, and we trace the cause to lightning-induced photochemistry. The following sections provide background with experimental details (Sect. 2), observations (Sect. 3), photochemical model results (Sect. 4), a discussion (Sect. 5), and a conclusion (Sect. 6).

2 Data sets

2.1 NPOL radar

The NASA polarimetric Doppler weather radar (NPOL) is an S-Band system operating at a frequency of 2.8 GHz (10 cm wavelength). It has horizontal and vertical beam widths of 1.4°. The antenna is a flat, passive array instead of the typical parabolic dish. The design allows the system to be transported easily and allows NPOL to operate in conditions with strong winds (e.g., minimum wind loading). One of the main

drawbacks of this design is that the signal deteriorates when the antenna is wet (Theisen et al., 2009). Therefore, the final quality-controlled dataset excludes periods when there is precipitation at the radar site.

For TC4, NPOL was deployed next to the Nittany Atmospheric Trailer and Integrated Validation Experiment (NATIVE) mobile laboratory near Las Tablas. NPOL operated almost continuously 16 July–12 August 2007, with the exception of the period 18:00 UTC 19 July–02:00 UTC 21 July. NPOL scanned with a temporal resolution of 10 min and spatial resolution of 200 m using a 12-tilt scanning strategy with elevation angles ranging from 0.7° to 23.3°. A volume scan with a maximum range of 150 km preceded each long-range (to 275 km) surveillance scan. NPOL-measured or derived quantities included standard radar parameters: radar reflectivity (DZ), Doppler velocity (VR), and spectral width (SW); and polarimetric parameters: differential reflectivity (ZDR), differential phase (PhiDP), specific differential phase (KDP), and cross correlation (corrHV) between horizontal and vertical polarizations. Nearly 3500 volume scans are available for studying the convective properties in and around Panama, a data set that includes a variety of interesting events, ranging from short-lived unorganized convection to long-lived mesoscale convective systems.

2.2 World wide lightning location network

In 2007 the World-Wide Lightning Location Network (WWLLN) (Rodger et al., 2006) consisted of approximately 25 sensors detecting lightning flashes at VLF frequencies of 3–30 kHz. WWLLN Director, Robert Holzworth, of the University of Washington provided near-real-time flash data (primarily cloud-to-ground or CG flashes) to NASA Goddard Space Flight Center (GSFC). Bucsela et al. (2010) estimated the detection efficiency of the WWLLN for total flashes (CG + intracloud or IC flashes) in the TC4 region (over open ocean near Costa Rica and Panama) through comparisons of flash rates from the Costa Rica Lightning Detection Network (CRLDN, which uses the same sensors as the United States National Lightning Detection Network, NLDN, see Cummins et al., 1998) and the Lightning Imaging Sensor (LIS) on the Tropical Rainfall Measuring Mission (TRMM) satellite for six storms. The mean detection efficiency was 0.22 ± 0.08, in reasonable agreement with, though somewhat higher than, the estimate of Rodger et al. (2006). There is some indication, however, that the detection efficiency is greater over the ocean than over the land in this part of the world (Lay et al., 2009).

2.3 OMI

OMI has been collecting data since its launch in July 2004 (Levelt et al., 2006). The instrument is a nadir-viewing spectrometer with a CCD-array having wavelength and spatial dimensions, the latter comprising 60 pixels across the flight track. The pixel area at nadir is $13 \times 24\,km^2$, although this value increases by approximately an order of magnitude near the edges of the track. Overpass time is ~13:45 local time in the tropics, improving the capability of OMI for observing afternoon convective events as compared with GOME and SCIAMACHY (which have morning overpass times).

Bucsela et al. (2006, 2008), Celarier et al. (2008), and Wenig et al. (2008) describe the retrieval algorithm for NO_2 from OMI. It employs a spectral fitting procedure to obtain NO_2 slant column densities (SCDs) from the OMI spectra. Vertical column densities (VCDs) result from dividing SCDs by air mass factors (AMFs), which are derived through radiative transfer calculations. The tropospheric component of the vertical column, including both pollution and lightning sources, is obtained by removing an unpolluted (here simply called "stratospheric") component, using a wave-2 analysis in narrow latitude bands. Because of the method used to derive it, the stratospheric VCD is contaminated by small amounts of tropospheric NO_2, which we remove in the present study using output from the GMI model (Duncan et al., 2007). The corrected stratospheric VCD differs from the uncorrected value by approximately 5%.

For the 5 August 2007 analysis, OMI NO_2 data provide estimates of $LtNO_x$ in the region near the Gulf of Panama. Bucsela et al. (2010) provide details of the procedure, but we outline the method briefly. The first step is the calculation of the tropospheric SCD due to $LtNO_2$, which is given by the total SCD minus the sum of the corrected stratospheric SCD and the tropospheric SCD due to sources other than lightning. This non-lightning tropospheric SCD is obtained from the OMI observations in the TC4 regions on days with a minimum of convective activity. In these calculations, all SCDs and VCDs are related through AMFs derived using radiative-transfer calculations and climatological NO_2 profiles. We convert the $LtNO_2$ slant column to a vertical column of $LtNO_x$ using a modified AMF that accounts for the vertical distribution of $LtNO_2$ and the photolysis ratio of $[NO_2]/[NO_x]$. The former is obtained from TC4 aircraft data, and the latter from model calculations. Beirle et al. (2009) describe a similar approach.

The uncertainties in the OMI estimate of $LtNO_x$ are dominated by uncertainties in the global stratospheric and local background concentrations. These are treated as systematic errors, as opposed to random errors. The pixel-scale errors include variations in cloud parameters, photolysis ratios and the local a priori NO_2 profile, and make a negligible contribution to the total error budget. Other more significant errors include the uncertainties associated with the size of the region of interest and the number of lightning strokes contributing to the observed $LtNO_x$. As a result, the overall uncertainty in this estimate is large, though comparable to uncertainties associated with the other $LtNO_x$ estimates described below.

2.4 Ozonesondes

Launched from the NATIVE facility, the electrochemical concentration cell (ECC) type (Komhyr, 1986; Komhyr et al., 1995) En-Sci 2Z ozonesonde instruments with 0.5% buffered, KI cathode solution provided O_3 profiles during TC4 at the Las Tablas site. The Jülich Ozone Sonde Intercomparison Experiment (JOSIE) found biases <5%, a precision of 3–5%, and an accuracy of 5–10% up to 30 km for such sondes (Smit et al., 2007). With a typical rise rate of ∼5 m/s and a measurement time constant of ∼25 s, the effective vertical resolution of O_3 features is ∼125 m (see also Smit et al., 2007). Most launches occurred from 12:00–15:00 local time (17:00–20:00 UTC) to coincide with the ∼13:45 local solar time overpass of NASA's Aura satellite (Schoeberl et al., 2006).

Vaisala RS80-15N radiosondes on each payload (described in Thompson et al., 2003, 2007a) measured pressure, temperature, and relative humidity (RH). Payloads also contained global positioning systems (GPS) that provided latitude, longitude, altitude, wind speed, and wind direction data. Comparisons of pressure altitude with GPS altitude provide validation of the pressure measurements. When pressure offsets occur, they are usually <2 hPa, meaning that tropospheric O_3 mixing ratios are adjusted <∼2% (<∼0.2% at the surface). Post-flight processing corrects pressure errors so that at burst altitude, pressure and GPS altitudes agree to within 200 m. For 7 of the launches during TC4, RH data above 300–500 hPa appear unreliable. All the ozonesonde data can be found at: http://physics.valpo.edu/ozone/tc4data.html.

Although each ozonesonde is internally calibrated before each flight, Fig. 1 shows a comparison of surface O_3 readings with pre-launch ozonesonde readings from the 23 flights with good O_3 data during TC4. The Thermo Electron Corporation (TECO) Model 49C Ozone Analyzer, using the United States Environmental Protection Agency standard measurement technique (EQOA-0880-047) and located on the NATIVE trailer (data at: http://espoarchive.nasa.gov/archive/arcs/tc4/data/native) trailer in Las Tablas, provided the preflight surface O_3 data. The mean bias (sonde – NATIVE) was -0.4 ± 1.2 ppbv, with a root mean square difference of 1.05 ± 0.76 ppbv.

We compare ozonesonde columns with OMI total column ozone (Bhartia, 2007; McPeters et al., 2008) for nearby overpasses (<50 km from launch site). To determine the ozone column from the ozonesonde data, we integrate ozone profiles to the burst altitude, then augment the column with either a constant mixing ratio assumption for the upper stratosphere or the Solar Backscatter Ultra-Violet (SBUV) balloon-burst climatology of McPeters et al. (1997). For the former case, the difference is 17.5 ± 3.8 DU, while for the latter, the difference is 16.7 ± 6.2 DU, with the sondes higher than OMI by ∼6%. These results are consistent with the finding that the Paramaribo SHADOZ station (5.8° N, 55.2° W) reports columns ∼10% higher than OMI (Thompson et al., 2007c).

3 Observations

Because of the large uncertainties associated with the determination of lightning flash rates from radar and satellite data, and because of the large uncertainties in the quantities important for the calculation of O_3 production from lightning flashes (e.g., ozone production efficiency, NO_x per stroke of lightning, the ratio of CG to intracloud (IC) flashes), we explore this event from the perspective of many observational data sets. In Sect. 3.1, we present the NPOL observations of the lightning flashes as this cell comes across the Azuero Peninsula. In Sect. 3.2, we present observations of the same event as seen in the WWLLN data. In Sect. 3.3, we present the corresponding NO_x data from the Aura OMI instrument. Finally, in Sect. 3.4, we present the in situ observations from the ozonesonde flight on 5 August 2007.

3.1 NPOL

NPOL observed a large convective system off the coast of Panama on 5 August 2007. The system developed during overnight hours in the Gulf of Panama and slowly propagated westward toward the Azuero Peninsula. NPOL data indicated that the precipitating area covered several hundred kilometers in the north-south direction and ∼100 km in the east-west direction, with the convective core having a mean area of 5300 ± 2400 km^2 between 09:00–17:00 UTC. The peak convection occurred ∼13:11 UTC. Figure 2 shows the reflectivity (DZ) field for 12:55–13:05 UTC. Reflectivity values ranged from about 0 dBZ in the lighter precipitation areas to a maximum of about 55 dBZ in the embedded convection.

Estimated wind velocities are derived from NPOL Doppler velocity field through a technique called volume velocity processing (VVP) (Boccippio, 1995). For the 5 August cell, the derived wind in the lower atmosphere was easterly at speeds on the order of 10 m/s. With each time step, however, moderate directional shear appeared, with directions fluctuating from southeast to northeast (in agreement with the ozonesonde observations, see Sect. 3.4 below).

This convective system generated a significant number of lightning strikes. Figure 2 indicates the location of flashes between 12:55 and 13:05 UTC detected by the WWLLN (see Sect. 3.3 below) are well correlated with areas active convection indicated by the NPOL data. We use radar reflectivity data from NPOL to estimate lightning flash rates using the parameterization of Futyan and DelGenio (2007), which predicts the total flash rate IC + CG = F (flashes/min/300 km^2) to be

$$F = 0.208(H_{17\mathrm{dB}} - H_{0^\circ\mathrm{C}})^{1.8} \quad (1)$$

Table 2. Flashes detected by the World Wide Lightning Location Network (WWLLN Flashes), estimated flashes using the WWLLN detected flashes and the network flash detection efficiency (WWLLN Flashes*), and flashes calculated from radar heights estimated by the NPOL radar (uncertainties in parenthesis) near the Gulf of Panama on 5 August 2007. WWLLN Flashes 2 refer to flashes detected in the region upwind of the DC-8 spiral on 5 August 2007. See text for details of each.

Hours (UTC)	WWLLN Flashes	WWLLN Flashes*	NPOL Flashes	WWLLN Flashes 2	WWLLN Flashes 2*
00:00–08:00	9	41 (15)	0	103	470 (170)
08:00–09:00	4	18.2 (6.6)	0	51	230 (84)
09:00– 10:00	36	163 (60)	9 (10)	26	118 (43)
10:00–11:00	61	277 (101)	0	9	41 (15)
11:00–12:00	34	155 (56)	44 (72)	13	59 (21)
12:00–13:00	174	791 (288)	240 (61)	13	59 (21)
13:00–14:00	160	727 (264)	450 (240)	0	0
14:00–15:00	92	418 (152)	670 (110)	0	0
15:00–16:00	6	27 (10)	600 (100)	0	0
16:00–17:00	0	0 (0)	240 (78)	0	0
17:00–18:00	1	4.5 (1.7)	11 (13)	0	0
18:00–19:00	2	9.1 (3.3)	1.7 (2.1)	5	22.7 (8.3)
19:00–20:00	9	41 (15)	4.3 (6.3)	0	0
20:00–24:00	150	682 (248)	108 (63)	34	155 (56)
Total 09:00–17:00	**563**	**2560 (440)**	**2300 (300)**	**61**	**277 (55)**
TOTAL	**738**	**3400 (500)**	**2400 (310)**	**254**	**1160 (210)**

where H_{17dB} is the storm-averaged height (km) of the 17dB radar-return signal and $H_{0\circ C}$ is the height of the 0 °C (freezing) level. From the ozonesonde data, we find $H_{0\circ C}$ is ∼4.5 km. From the radar data, we determine hourly averages of H_{17dB} and the area of the storm. Table 2 shows the resulting hourly flash estimates for 5 August. During the period from the genesis of the cell to the final ascent of the balloon (09:00–17:00 UTC), this parameterization predicts a total of 2300 ± 300 flashes.

We can use the NPOL-derived flash data to estimate the photochemical lightning production of O_3 ($LtpcO_3$) from LtNO. Estimates of LtNO vary widely (Pickering et al., 2009; Huntrieser et al., 2008; Koike et al., 2007; Hudman et al. 2007; Drapcho et al., 1983) from a low of 43 moles/flash (Skamarock et al., 2003) to a high of 1100 moles/flash (Price et al., 1997, Winterath et al., 1999). Pierce (1970) and Prentice and Mackerras (1977) estimate the ratio of IC flashes to CG flashes for ∼8° N to be 6.5–8.0. Estimates of the NO production efficiency of IC-to-CG flashes varies from 0.1 (Price et al., 1997) to 1.4 (Fehr et al., 2004). Lin et al. (1988) estimate the production of 30 moles of O_3 per mole of NO_x, (i.e., an ozone production efficiency, OPE, of 30) in box model studies of surface O_3 pollution while more recent studies find OPE in the range 4–12. For example, Shon et al. (2008) found an OPE of 4.5 for air downwind of an industrial complex air in Mexico and 8.5 for free tropospheric marine air; Wood et al. (2009) found an OPE of ∼7 over the course of a day at a mountain observatory near Mexico City; and Zaveri et al. (2003) used aircraft and surface observations during the Southern Oxidant Study, finding OPEs increased with plume age from ∼2–5.6. (Note: for our calculations of $LtpcO_3$, we scale the OPE to account for the limited 2-h period between the first and final ascent and assume that enough sunlight was available on the edge of the cell to drive the photochemistry).

Using a Monte Carlo approach to combine the various parameters cited above, we estimate $LtpcO_3$ of $(4.2 \pm 4.0) \times 10^6$ moles from this cell. The large uncertainty in this estimate owes to the remaining high uncertainty in all of the quantities that go into the calculation. Recalculating with values that we feel are most representative of the conditions for this cell (tropical, marine, etc.: OPE = 2; moles NO/flash = 227 as suggested by Bucsela et al. (2010); IC:CG NO production efficiency = 1), we determine our best estimate of $LtpcO_3$ to be 1.0×10^6 moles using on the NPOL-based lightning flash rates.

If we assume O_3 is produced directly from coronal discharges, estimated from the number of lightning strikes ($LtdO_3$) at 300–3000 moles/flash, as in Minschwaner et al. (2008), we predict $(3.7 \pm 1.8) \times 10^6$ moles of O_3 for the flashes between 09:00–17:00 UTC. Since the ozonesonde observations suggest that the O_3 production was ongoing during at least the 108-min period after launch, only the $LtdO_3$ after launch is relevant. Therefore, if we restrict our calculation to the flashes during the two-hour period after launch (see Table 2), we find possible $(1.39 \pm 0.70) \times 10^6$ moles of $LtdO_3$.

3.2 WWLLN

WWLLN reported frequent lightning in association with the convective cell over the Gulf of Panama on 5 August. Table 2 summarizes the number of flashes per hour detected in the box defined by the latitude range 7.25°–8.75° N and longitude range 78.75°–81.25° W, the region of the Gulf of Panama through which the convective cell passed. Figure 2 shows good correlation between the locations of the lightning flashes and the areas of active convective seen by the NPOL radar for 12:55–13:05 UTC. Notably, the CRLDN observed few if any lightning flashes over the Gulf of Panama on this day. Given the spatial distribution of lightning flashes observed by the CRLDN (not shown), it appears that the Gulf of Panama fell in a shadow of the network.

Using the WWLLN flash data between 09:00–17:00 UTC, we can estimate the associated total $LtpcO_3$, as we did for the NPOL data above with one further modification. Bucsela et al. (2010) estimated lightning detection efficiency of 0.22 ± 0.08 for the WWLLN in the TC4 region. Accounting for this factor, we find 2560 ± 930 flashes between 09:00–17:00 UTC, in reasonable agreement with the NPOL estimate of 2300 ± 300 flashes. (Hour-by-hour estimates of the efficiency corrected WWLLN flashes can also be found in Table 2.)

Using a Monte Carlo approach to combine the factors in Sect. 3.1 above with the WWLLN flash estimate, we find $(3.3 \pm 4.5) \times 10^6$ moles of $LtpcO_3$, with our best estimate of 1.2×10^6 moles (using values associated with conditions more likely to be found in the present case, as we did for the NPOL calculation above), consistent with the NPOL estimate.

If we assume direct production of O_3 via coronal discharges at 300–3000 moles/flash, as in Minschwaner et al. (2008), and use the WWLLN efficiency corrected lightning strikes, we project $(4.2 \pm 2.2) \times 10^6$ moles of $LtdO_3$ for the flashes between 09:00–17:00 UTC. Although the cloud parameterization used to estimate lightning frequency from the NPOL data (see Table 2) suggests lightning continued during the sonde oscillation period (15:00–17:00 UTC), the WWLLN suggests little-to-no lightning during this period. This mechanism, therefore, is not indicated by the WWLLN data for post-launch O_3 production.

3.3 OMI NO_2

It is difficult to discern the $LtNO_2$ signal from an examination of Level 2 OMI tropospheric NO_2 and cloud fraction data products that result from the standard retrieval conducted at NASA Goddard Space Flight Center (Bucsela et al., 2006), in part because the Level 2 data have not been cloud screened. With reprocessing that includes removing an estimate of background NO_2 and applying an air mass factor more appropriate for convective outflow (Bucsela et al., 2010), the $LtNO_2$ becomes more evident. Fig. 3 shows

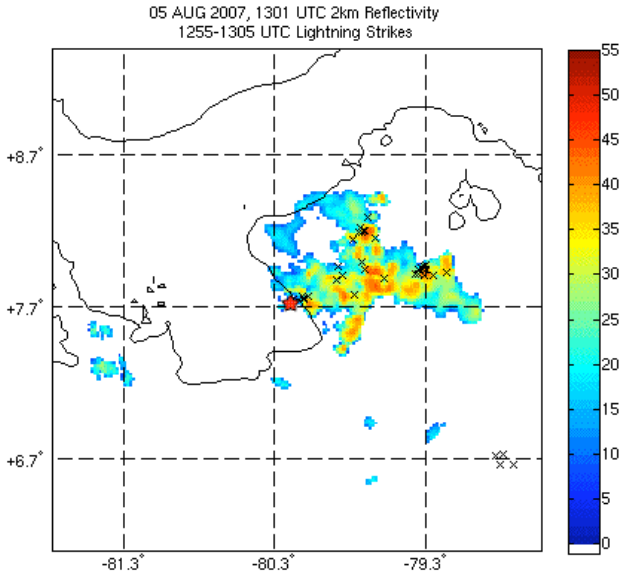

Fig. 2. Low-level (0.7 elevation) PPI images of convection observed east of NPOL at 13:11 UTC 5 August 2007. The color scale has units of radar reflectivity (dBZ). Each "X" marks the location of a detected WWLLN lightning strike. The red star marks the location of Las Tablas.

a map of the $LtNO_x$ field near the Gulf of Panama on 5 August 2007 after reprocessing (considering the NO_x to NO_2 ratio at cloud-outflow levels). The boxed area ($\sim$54 000 km^2) contains 1020 ± 860 kmol $LtNO_x$, which would result in $(1.2–8.9) \times 10^6$ moles of O_3 (depending on the OPE selected). If we scale this estimate to the size of the core of the convective cell observed on the NPOL radar (average area of $\sim$5300 km^2 from 09:00–17:00 UTC), the estimated $LtpcO_3$ becomes $(1.2–8.6) \times 10^5$ moles, with a best estimate of $(2.0 \pm 1.7) \times 10^5$ moles, whereas if we scale it to match the area of flashes detected by the WWLLN ($\sim$46 000 km^2), we find a range of $(1.0–7.6) \times 10^6$ moles with a best estimate of $(1.7 \pm 1.5) \times 10^6$ moles. Scaling by the larger area of the WWLLN estimate results in the best agreement with the NPOL and WWLLN $LtpcO_3$ estimates detailed above. While the uncertainties are large, the values appear to be above background.

3.4 Ozone profiles

The ozonesonde launch on 5 August occurred at 15:05 UTC to coincide with the scheduled arrival of the NASA aircraft in the Panama area. At the time of launch, rain fell as part of the convective cell that had just moved ashore from the east, although ground observers reported no visible lightning. The surface temperature was $\sim$24°C with RH of 96% and a surface pressure of $\sim$1003 hPa.

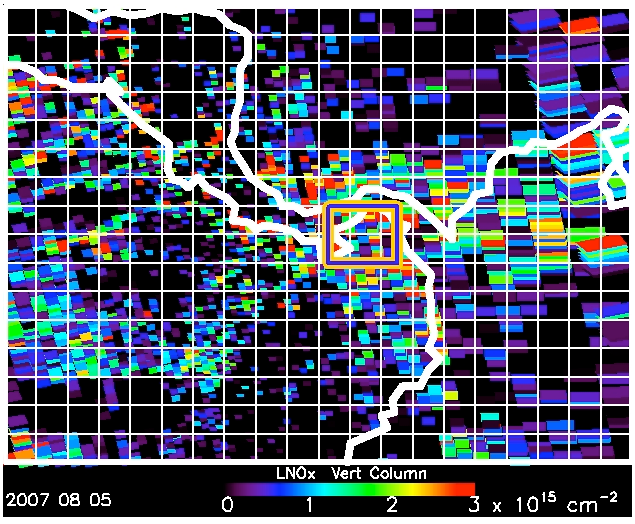

Fig. 3. Gridded (1° × 1°) OMI lightning NO_x in the Panama area on 5 August 2007. The larger region was used for the first estimate, while the smaller boxed region in the Gulf of Panama was used for the second estimate (see text).

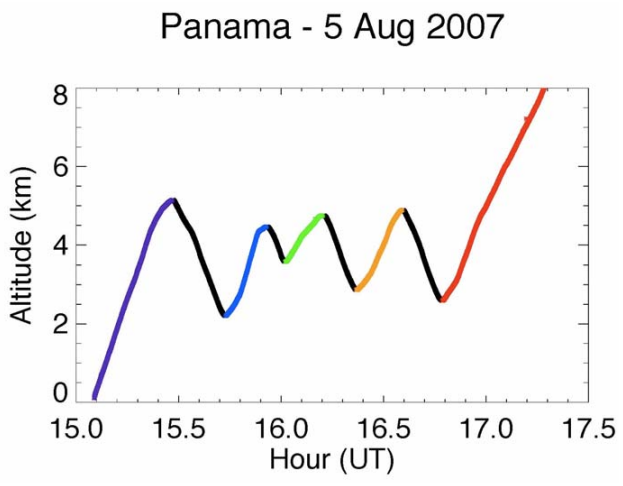

Fig. 4. The altitude vs. time of the ozonesonde flight on 5 August 2007 from Las Tablas, Panama shows the balloon oscillating 5 times between ∼2.5 and ∼5.1 km. The color coding of each ascent will be used in successive plots to identify changes with time of other measured parameters.

About 20 min into the flight, the balloon reached 5.1 km and began to descend. About 15 min later, it began to ascend again. Between launch and ∼17:00 UTC, the balloon oscillated up and down through the air mass between ∼2.5 and ∼5.1 km five times, as shown in Fig. 4. (Note: each ascent is color-coded so subsequent figures can be analyzed more easily.) Although the detailed explanation for this behavior is beyond the scope of this paper (see Morris, 2011), it appears to be a combination of downdrafts on the southern side of the westward-moving convective cell (based on NPOL radar data) and changing mass due to repeated condensation/evaporation of water and freezing/melting of ice on the surface of the balloon.

Figure 5 shows the O_3 concentrations measured on each ascent. Over the ∼2 h between the original ascent and the final ascent, O_3 in the layer between ∼2.5 and ∼5.1 km increased 4–12 ppbv, with a mean increase of 7.9 ± 4.7 ppbv. Integrating the change in O_3 between the first and last profiles from 2.55–5.11 km (the range of the oscillation), and assuming uniform production across the area of the storm (5300 ± 2400 km^2 as indicated by the NPOL data from 09:00–17:00 UTC) in this layer, we find a potential of $\sim 3.0 \times 10^6$ moles of O_3 (with ∼50% uncertainty) created as part of this cell, a number that agrees within roughly a factor of two with the best estimates from the lightning data (see Sects. 3.1 and 3.2) and the OMI data (see Sect. 3.3 above). We note that the estimates from the lightning data and from OMI represent the total $LtpcO_3$ throughout the cloud, whereas our sonde estimate is based only on the enhancements in the 2.5–5.1 km layer.

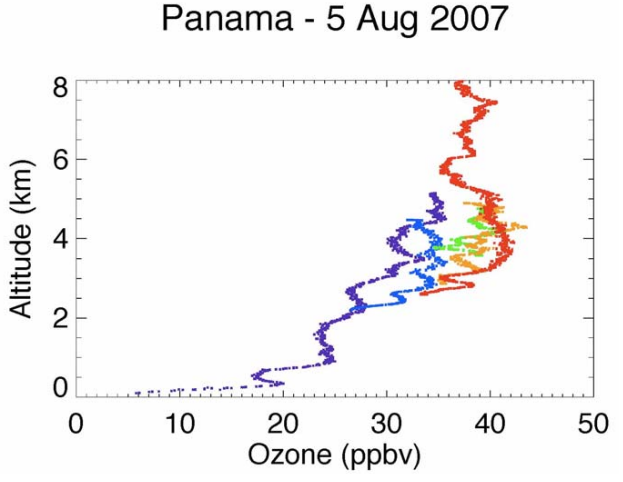

Fig. 5. Ozone vs. altitude on the ascents as the balloon oscillated on the 5 August 2007 flight, with color coding to match the ascents identified in Fig. 4.

Geostationary Operational Environment Satellite (GOES) data indicate cloud top temperatures consistent with heights of 14–15 km as the cell developed over the Gulf of Panama, descending to 11–12 km as the cell dissipated when moving ashore. Moderate-resolution Imaging Spectrometer (MODIS) data for this cell suggest the cloud tops reach 10–12 km. Both satellite data sets indicate the clouds reached altitudes far above the top of the layer in which the balloon oscillated. To get a better estimate of LtO_3 throughout the cloud and estimate changes in O_3 above 5.1 km, therefore, we use the O_3 data from the DC-8 flight around

the Gulf of Panama on 5 August. The mean DC-8 in situ O_3 profiles before 17:17 UTC and after 17:17 UTC can be seen in Fig. 6. Figure 7 shows the locations of the "before"/"after" data points, with the former marked by green stars and the latter by green diamonds. If we integrate the difference between the final ozonesonde ascent profile and the mean aircraft profiles (before and after 17:17 UTC) from 2.5–12.0 km, we find 4.2×10^6 and 3.1×10^6 moles, respectively. Using the combination of the in situ DC-8 measurements and the ozonesonde data, we find that 70–97% of the ozone molecules were created in the layer in which the balloon oscillated (i.e., 2.5–5.1 km).

The DC-8 differential absorption lidar (DIAL) observations, shown as the small colored dots in Fig. 6, provide evidence for higher O_3 downwind of convection as compared to observations upwind in clear-sky regions around the Gulf of Panama. The colors are coded to match the locations of these observations along the flight track shown in Fig. 7. Integrating the upwind-downwind differences from 1.6–8.5 km, we find an increase (post minus pre) of 1.3×10^7 moles of O_3, with roughly two-thirds of this change occurring between 1.6–6.0 km.

Returning to the ozonesonde observations, the total change in O_3 as observed by the balloon is given by

$$\frac{d[O_3]}{dt} = \frac{\delta[O_3]}{\delta t} + \boldsymbol{v} \cdot \boldsymbol{\nabla}[O_3] \quad (2)$$

where the first term represents in situ photochemical production (loss) and the second term represents changes due to advection. If the balloon had remained in the same air parcel within the cloud or if no wind sheer existed over the vertical range of oscillation, we could assume that the observations were Lagrangian, meaning the advection term would vanish. Figure 8 shows the wind speeds and directions on each ascent of the balloon as determined from on board GPS data. Because of the vertical wind shear within the cell (seen by NPOL and in the balloon data), the advection term (resulting from the difference between the trajectories of the balloon and the air parcels in which observations were taken) may be non-negligible, so we investigate further below.

Table 3 shows the calculated differences between the GPS-recorded balloon positions and the estimated subsequent positions of the air masses sampled on the first ascent at three levels (2.75, 3.75, and 4.75 ± 0.15 km). To make these estimates, we calculated trajectories based upon GPS wind speed and direction vertically averaged in each of the three layers on successive ascents. We multiplied the resulting u (east-west wind) and v (north-south wind) values by the time difference between successive ascents to get longitude and latitude displacements. Since the balloon did not oscillate through all three layers each time, the table contains some "No data" entries. These calculations suggest separations of 15–30 km between the originally- and finally-sampled air masses, providing a constraint on the horizontal scale of potential O_3 gradients.

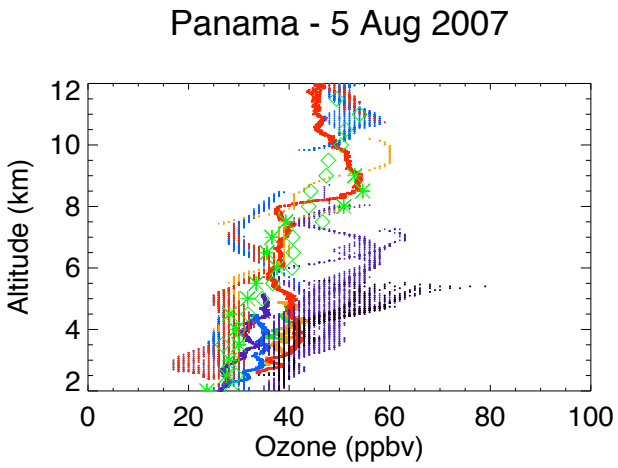

Fig. 6. Ozone profiles on 5 August 2007 in the Gulf of Panama region from sonde (thick colors), DC-8 DIAL (colored dots), and mean DC-8 in situ (green diamonds before 17:17 UTC and green stars after 17:17 UTC). See text for details.

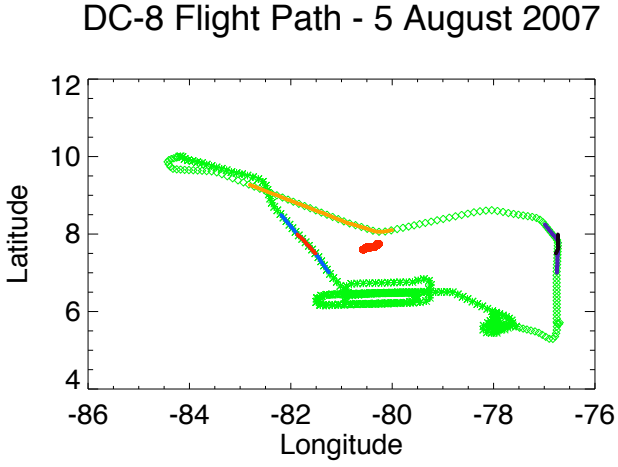

Fig. 7. DC-8 flight path with green stars marking the flight path prior to 17:17 UTC and the green diamonds marking the flight path after 17:17 UTC. The colored dots superimposed on the flight path correspond to DC-8 DIAL measurement locations, with the color-coding to match the profiles seen in Fig. 6.

Figure 9 shows the change in O_3 with time as a function of altitude, calculated as the difference between the O_3 at a given altitude as measured on each ascent with that measured on the first ascent. Changes of 3–10 ppbv/hr are derived, with the highest rates at 2.5–3.0 km between the first and second ascents, and at 3.5–4.5 km between the first and third ascents. We note from Table 3 that for the former case, the balloon is located about 5 km upwind from the original air mass, somewhat farther from the center of the storm as it comes ashore. For the latter case, the balloon is located about 13 km downwind of the original air mass, closer to the center of the cell.

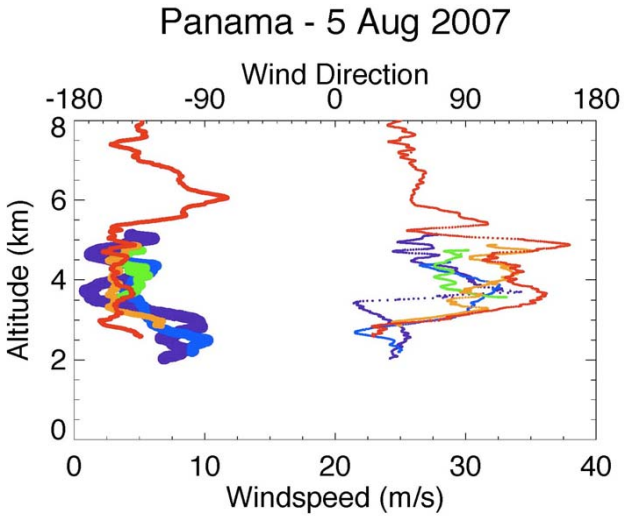

Fig. 8. Wind speed (thick) and direction (thin) as determined from the ozonesonde GPS data. The balloon moved through a region of vertical shear, resulting in the separation of the balloon trajectory from the trajectories of the air masses the sonde sampled. See text and Table 3 for further details.

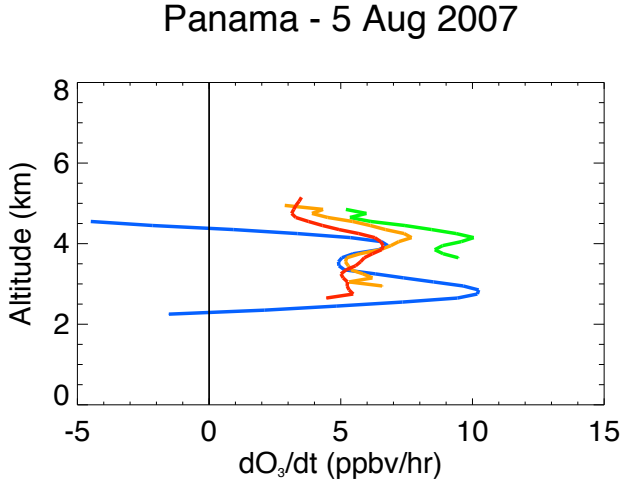

Fig. 9. Calculated dO_3/dt vs. altitude for the ascents of the flight on the 5 August 2007 flight, with color coding to match the ascents identified in Fig. 4. See text for details.

Since both profiles suggest somewhat large O_3 changes with time, with one being upwind and the other being downwind of the original air masses, it seems likely that the advection term over these spatial scales is relatively small.

One last component of the advection term to investigate is the vertical term. While some of the change in O_3 is due to descent, most of the change appears to be due to other factors. First, the original ascending profile in Fig. 5 (purple) joins with near perfect continuity the final ascending profile between 5 and 5.5 km, suggesting the O_3 enhancements

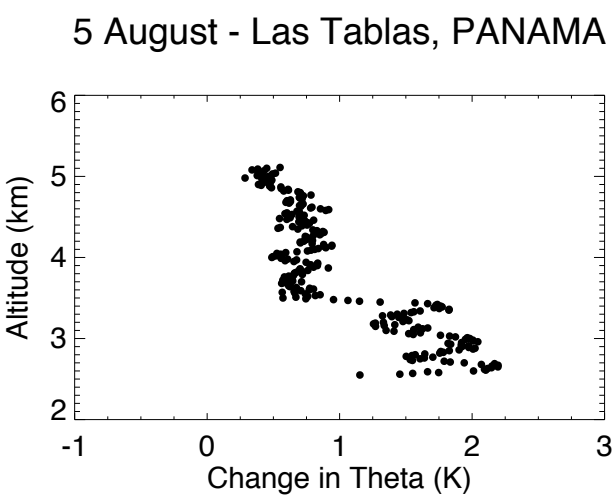

Fig. 10. The change in potential temperature from the first to the last ascent vs. altitude for the flight of 5 August 2007.

are not due to air descending from above 5.5 km. Second, Fig. 10 shows the change in potential temperature (theta) between the first and final ascent as a function of altitude between 2.55–5.11 km, with warming between 2.55 and ~3.40 km of 1.25–2.25 K, and between 3.4–5.11 km of 0.25–1.0 K. If we assume that the change in theta in the lower layer is due solely to descent, the air found in the 2.55–3.40 km layer on the last pass was originally between 3.09–3.55 km. The mean O_3 in this layer (defined by theta) on the first pass was 32.1 ± 1.3 ppbv while on the last pass, it was 37.9 ± 2.2 ppbv, a difference of 5.8 ± 2.6 ppbv. If we assume no descent at all, the mean O_3 in this layer (defined by altitude) was 29.5 ± 1.9 ppbv on the first pass, a difference of 8.4 ± 2.9 ppbv. Thus, we attribute 2.6 ± 3.9 ppbv (~31%) of the change to descent of air between the first and last ascents, with air descending at an average rate of 6.2 cm/s. Reducing the observed change in O_3 of 4–12 ppbv over ~108 min (the time between the first and final ascent) by the 30% due to descent, the balloon data project 1.5–4.6 ppbv/hr change in O_3.

Figure 11 shows O_3 as a function of theta rather than height for the first and last ascents. Integrating the change in O_3 as a function of theta between 311.75–320.00 K, and assuming the cell size as before, we find an increase of 2.5×10^6 moles of O_3, agreeing within roughly a factor of two with the estimates from the lightning data detailed above.

To establish characteristics of the large scale flow, we calculated back trajectories from 2.75–4.75 km using both the Hysplit model (Draxler and Rolph, 2010) using Global Data Assimilation System (GDAS) meteorological fields (horizontal resolution of 1° latitude × 1° longitude) and a kinematic version of the NASA Goddard Space Flight Center trajectory model (GTM, Schoeberl and Sparling, 1995) using National Centers for Environmental Predication (NCEP) reanalysis meteorological fields (horizontal resolution of 1°

Table 3. Balloon trajectory and estimated air mass trajectories at three different altitudes within the 2.5–5.1 km layer in which the balloon oscillated. "No data" are reported when the balloon did not oscillate through the level of the air mass trajectory calculation. The "Direction" column indicates the compass heading from the balloon location to the estimated air mass location. Color-coding matches that for the balloon data shown in Figs. 4, 5, 8, 9, and 11. See text for details.

Trajectory Altitude (km)	Time from launch (s)	Balloon lat (deg)	Air mass lat (deg)	Balloon lon (deg)	Air mass lon (deg)	Separation (km)	Direction (deg)
	614	7.734	7.734	−80.269	−80.269	0.000	0
	2555	7.677	7.661	−80.337	−80.382	5.246	250
2.75 km	no data	no data	no data	no data	no data	no data	no data
	4629	7.660	7.597	−80.418	−80.492	10.816	230
	6208	7.654	7.550	−80.463	−80.551	15.103	220
	859	7.724	7.724	−80.277	−80.277	0.000	0
	2766	7.674	7.683	−80.346	−80.262	9.320	84
3.75 km	3459	7.671	7.657	−80.374	−80.260	12.672	97
	5010	7.654	7.605	−80.431	−80.261	19.494	106
	6535	7.655	7.565	−80.469	−80.235	27.614	111
	1134	7.722	7.722	−80.284	−80.284	0.000	0
	no data	no data	no data	no data	no data	no data	no data
4.75 km	3956	7.667	7.635	−80.393	−80.307	10.116	111
	5335	7.658	7.582	−80.440	−80.300	17.591	118
	6806	7.659	7.544	−80.476	−80.269	26.130	119

latitude × 1° longitude and a 6-h time resolution). The results from both models suggest that air masses between 2.75 and 4.75 km moved across the Gulf of Panama from the ENE to Las Tablas over the 8 h prior to the balloon observation, consistent with the motion of the cell seen in the NPOL radar data. The trajectory data, therefore, suggest that the air mass was not a mixture of air from vastly different source regions.

4 Photochemical modeling

In a effort to simulate the O_3 changes observed by the 5 August 2007 ozonesonde, we ran a zero-dimensional photochemical box model with Regional Atmospheric Chemical Mechanism (RACM, Stockwell et al., 1997) to calculate the concentrations of radicals and other reactive intermediates. Rate coefficients of the reactions in RACM were updated by Jet Propulsion Laboratory (JPL) data evaluation (Sander et al., 2006) as applicable. The model was constrained by a set of 1-min resolution merged observations of temperature, pressure, H_2O, O_3, CO, NO, NO_2, HNO_3, NMHC, ethanol, acetone, MACR, MVK, and benzene from NASA DC-8 aircraft at 16:45–17:00 UTC on 5 August 2007. During this time period, the aircraft was spiraling downward from 5.2 to 0.3 km near 5.7° N and 78.0° W, in a clear-sky region to the southeast of the active region of convection in which the balloon measurements occurred. Unmeasured photolysis frequencies were calculated for clear sky condition from the Tropospheric Ultraviolet and Visible (TUV) model (http://www.acd.ucar.edu/TUV) or based on the solar zenith angle equations in Jenkin et al. (1997) and then scaled by the photolysis frequency of NO_2 calculated from the NCAR CCD Actinic Flux Spectroradiometers (CAFS) measurements made on the NASA WB-57 aircraft that flew in the vicinity of active convection around the same time as the DC-8. The model was run with the FACSIMILE software (MCPA Software Ltd.) for sufficient time to reach instantaneous steady state of the intermediates.

The instantaneous net O_3 production, $P_{net}(O_3)$, can be calculated by

$$\begin{aligned} P_{net}(O_3) &= P(O_3) - L(O_3) \\ &= k_{NO+HO_2}[NO][HO_2] + \Sigma k_{NO+RO_2 i}[NO][RO_2] \\ &\quad - k_{OH+NO_2+M}[M][NO_2][OH] - k_{O1D+H_2O} \\ &\quad [O^1D][H_2O] \\ &\quad - k_{HO_2+O_3}[HO_2][O_3] - k_{OH+O_3}[OH][O_3], \end{aligned} \quad (3)$$

where the various k's represent the rate coefficients of the corresponding reactions associated with the production and loss of O_3. The resulting calculated net ozone production as a function of altitude is shown in Fig. 12a, with a mean value of 0.84 ppbv/hr between 2–5 km. Because this aircraft spiral occurred in a region with much less convective activity than the cell in which the ozonesonde made its measurements, we performed four additional model runs with NO_x concentrations 150%, 200%, 300% and 500% of those detected in

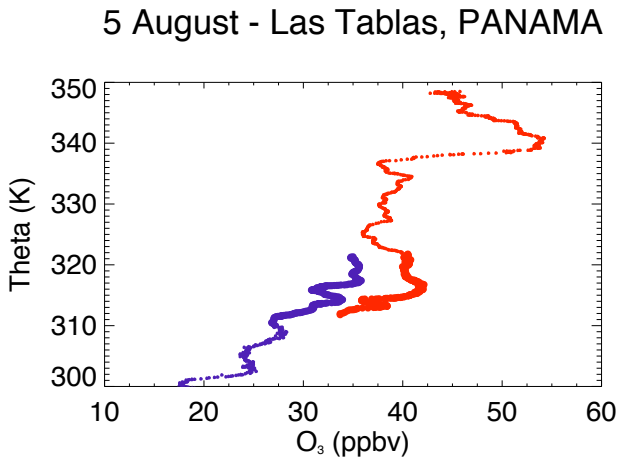

Fig. 11. Ozone vs. potential temperature for the first and last ascents of the flight of 5 August 2007 shows that the changes cannot be due to descent of the air mass alone.

this spiral (Fig. 12a). The runs resulted in 2–5 km averaged P_{net} (O_3) of 1.5, 2.2, 3.3, and 5.3 ppbv/hr, respectively.

Table 2 summarizes the WWLLN flash detection for 5 August in a box defined by 5.0–6.5° N, 75.5–78.5° W, a box of roughly the same area as used for the analysis of the convective cell in the Gulf of Panama discussed above. This box is located upwind of the area of the DC-8 spiral on 5 August. Hysplit trajectory calculations (not shown) suggest that air sampled by the DC-8 in its spiral would have been located in this box earlier in the day. The WWLLN data indicate that the air mass sampled during the DC-8 spiral saw only ∼10% as much lightning from 09:00–17:00 UTC and only ∼34% as much lightning for the entire day as the area near the convective cell. Increases of NO_x by a factor or 2–3 for use in modeling LtpcO_3, therefore, are reasonable, if not conservative.

Figure 12b examines the sensitivity of the calculated net ozone production rates on the photochemical rate constants. DeCaria et al. (2005) suggest a linear scaling of the clear sky photolysis rate constants using adjustment factors ranging from 0.1 at the base to 2.0 at the top of a very dense cloud, and from 0.4 at the base to 1.7 at the top of a dense cloud. Because we do not know the precise structure of the cloud in which the balloon oscillated, we perform a sensitivity study, scaling the photolysis rates by the amounts suggested by DeCaria et al. (2005) and using the 200% NO_x case described above. The average net ozone production for the 0.1, 0.4, 1.7, and 2.0 cases are 0.83, 1.5, 2.6, and 2.7 ppbv/hr respectively.

The Cloud Physics Lidar (CPL, McGill et al., 2004) and Cloud Radar System (CRS, Hlavka et al., 2010[1]) data from the DC-8 flight on 5 August (shown in Fig. 10 of Thompson et al., 2010) suggest some structure topping out in the 4–6 km altitude range, near the top of the range of the balloon oscillation. The production rates in the cloud sampled on 5 August, therefore, should move from the 0.1 or 0.4 scaled curves in Fig. 12b near 2.5 km toward the 1.0 to 2.0 scaled curves near 5.0 km, resulting in estimated production rates of 1.0–1.7 ppbv/hr near 2.5 km to 1.3–1.6 ppb/hr near 5.0 km. Thus, the photochemical model results are consistent with ∼1.0–2.5 ppbv/hr in the 2–5 km altitude range sampled by the oscillating balloon. (We note that by using the 500% NO_x case for this sensitivity analysis, we find ∼2.1–4.7 ppbv/hr at the cloud base and ∼3.5–4.5 ppbv/hr near 5.0 km, results that are quite consistent with the rates calculated from the balloon data above).

To support the use of enhanced NO_x in the photochemical model, we examine aircraft NO data, gathered using a chemilumenescence technique (Fontjin et al., 1970; Pearson and Stedman, 1980), and NO_2 data, gathered using the thermal dissociation – laser induced fluorescence technique (Thornton et al., 2000), from all DC-8 flights during TC-4.

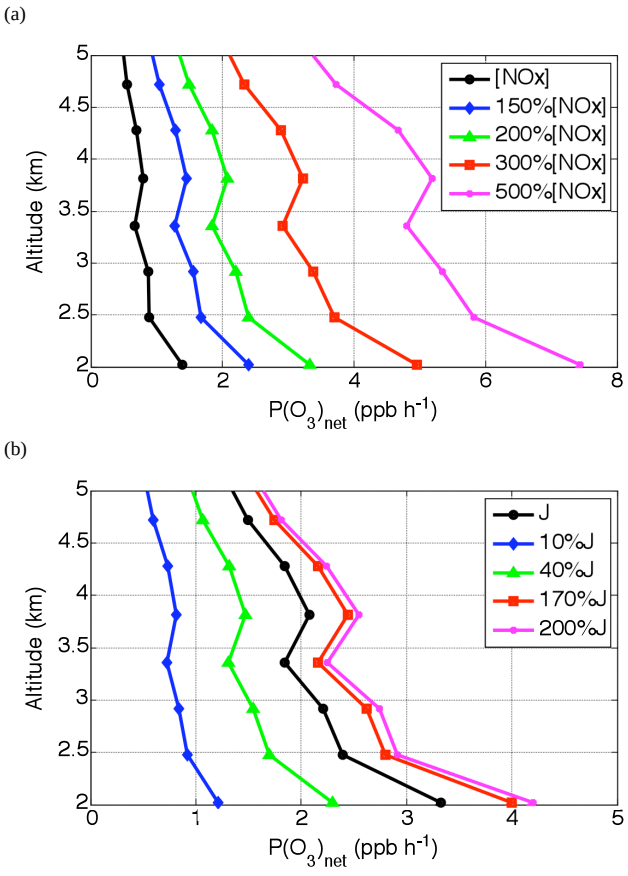

Fig. 12. Calculated ozone net production $P_{net}(O_3)$ within the altitude of 2–5 km based on the modeling results from the aircraft data at UTC 16:45–17:00 on 5 August 2007 with initial and controlled **(a)** NO_x concentrations and **(b)** photolysis rates (J values) with 200%[NO_x] case.

[1]Hlavka, D., Tian, L., Hart, W., Li, L., McGill, M., and Heymsfield, G.: Vertical cloud climatology during TC4 derived from high-altitude aircraft merged lidar and radar, unpublished manuscript, 2010.

These data are shown in Fig. 13 and only measurements recorded at least 10 min. after take-off, at most 10 min. before landing, and at least 50 km away from the airport in Alujuela, Costa Rica (10.0° N, 84.2° W) are included in the plot. Relatively high values of NO_x can be found throughout the troposphere. Tables 4 and 5 summarize all occasions when the NO and NO_2 concentrations exceeded 1.0 ppbv. We note two of these occasions in particular: (1) on 21 July 2007, a peak of 1.0–3.1 ppbv of NO is observed over the Carribean Sea between 3.7–6.2 km; (2) on 29 July 2007, a peak of 1.0–1.5 ppbv of NO between 6.3–7.4 km and a peak of 1.0–1.8 ppbv of NO_2 between 5.5–7.4 km is observed over the Pacific Ocean. Observation 1 occurred as the aircraft was descending after passing through an area of fresh convection, as indicated by the GOES IR data (anlger.larc.nasa.gov/tc4) for 21 July 2007. Observation 2 occurred just off the west coast of Costa Rica immediately following take-off. The aircraft encountered a region of fresh convection, as indicated by the GOES IR data for 29 July 2007. These two examples from the TC4 aircraft data support the possibility that NO_x production associated with fresh convection can be observed in the mid-troposphere.

5 Discussion

This work has presented a unique ozonesonde profile over Las Tablas, Panama on 5 August 2007. The balloon initially ascended on the southern side of a dissipating convective cell as it came ashore from the east. Between 09:00 and 17:00 UTC, WWLLN data indicate 563 flashes (∼2600 flashes accounting for the lightning detection efficiency of this network) in and around the Gulf of Panama, while estimates of lightning flash rates using NPOL radar height data result in ∼2300 flashes associated with this cell. The ozonesonde oscillated 5 times between ∼2.5 and ∼5.1 km for ∼108 min and measured 4–12 ppbv O_3 increases. Examination of the meteorological data gathered on the sonde flight suggests that ∼30% of the increase may be due to descent of higher O_3 from above. As a result, we calculate LtO_3 from the balloon measurements of 1.5–4.6 ppbv/hr. Using data gathered on DC-8 flight in the Gulf of Panama region on 5 August 2007, we initialized a run of the RACM to evaluate $LtpcO_3$ from the background conditions. Although the aircraft samples used to initialize the RACM run came from a region with only 10–34% as many lightning flashes, the base run showed a $LtpcO_3$ of 1.5 ppbv/hr between 2–5 km. Increasing NO_x by a factor of 2–3 and compensating for changes in photolysis rates due to cloud cover, as suggested by DeCaria et al. (2005), led to net $LtpcO_3$ of 1.0–2.5 ppbv/hr (increasing NO_x by a factor of 5 yields net ozone production rates of 2.1–4.7 ppbv/hr). The RACM model results, therefore, indicate that most of the $LtpcO_3$ observed by the ozonesonde can result from known photochemistry.

A number of previous studies have suggested that strong O_3 increases are seen at higher altitudes downwind of convective activity (see Table 1 for a summary of previous findings). For example, DeCaria et al. (2005) found O_3 production of 10 ppbv/day near 9 km, and Pickering et al. (1996) and Thompson et al. (1997) found 7–8 ppbv/day in the 8–12 km.

Other studies suggest O_3 losses due to titration by NO near 5 km in association with convective cells, including 6–8 ppbv losses found in Ridley et al. (2006), 9 ppbv losses during a convective event in Europe at 5.5 km reported by Ott et al. (2007), and maximum O_3 losses at 5 km during a storm in the tropical Pacific reported by Salzmann et al. (2008).

But numerous previous studies also have reported large increases in O_3 in the lower troposphere. Dickerson et al. (1987) found a peak in O_3 at 5 km in association with convective activity, while Pickering et al. (1990) suggest the highest potential O_3 production of 7–17 ppbv/day below 5 km. Viewed in this context, our ozonesonde observations provide evidence for this layer of enhanced O_3 in the lower troposphere.

The rapid increase of O_3 seen in our sonde data may suggest that much of the O_3 production occurs soon after daylight returns to the air mass affected by the cell rather than over the course of a day, a hypothesis consistent with the laboratory work of Franzblau (1991, see his Fig. 2 which shows rapid recovery of O_3 in <10 min. when a UV lamp illuminates a controlled chamber after electrical discharges result in loss of O_3 through reactions with $LtNO_x$). Although our balloon payload contained no instruments with which direct measurements of radiation could be made, the meteorological observations from the ozonesonde flight are consistent with increasing radiation at 2.5–5.1 km over the time of the oscillations. In particular, the sonde reported higher temperatures (by 0.92 ± 0.46 °C) and lower humidity (by 9.2 ± 4.8%) on the final ascent as compared to the initial ascent between 2.6 and 5.1 km, both of which are consistent with increased sunlight. This explanation also is consistent with Ott et al. (2007), who reported 9 ppbv losses of O_3 during a storm with large amounts of $LtNO_x$, but 5 ppbv/day production of O_3 downwind at 5.5 km.

Significant changes in the lower free tropospheric O_3 associated with convective activity are consistent with the lower portion of the C-shaped $LtNO_x$ profile of Pickering et al. (1998), which shows 15.9% of the LtNOx below 5 km, and the updated profiles of Ott et al. (2010), which shows 14.7% of $LtNO_x$ below 5 km. While the ICARTT data shown in Hudman et al. (2007) do not indicate a significant enhancement of NO_x in the 2–6 km altitude range, the DC-8 did not sample in this altitude range near convective activity; nevertheless the higher variability in NO_x and corresponding lack of a similar increase in variability in the CO data at 3.5 km (see their Fig. 3) may be explained by lower tropospheric $LtNO_x$. As pointed out by Ridley et al. (2004), for cases in which CG flashes occur outside of the convective core or in regions of the convective cell influenced by downdrafts,

Table 4. Measurements of NO >1 ppbv, >50 km away from Alajuela, Costa Rica airport (10.0° N, 84.2° W) from DC-8 flights during TC4. Enhanced NO < 8 km are highlighted orange over Columbia, blue over open water, and yellow over the west coast of Costa Rica.

Date	Altitude (km)	Latitudes	Longitudes	NO (ppbv)
21 Jul 2007	10.7	4.3° N	76.1° W	1.0–1.1
21 Jul 2007	4.6–6.4	4.0°–4.4° N	73.4°–73.9° W	1.0–1.8
21 Jul 2007	0.5–0.6	4.2° N	73.6° W	1.3–2.5
21 Jul 2007	10.9	10.3°–11.5° N	75.6°–77.9° W	1.0–2.1
21 Jul 2007	3.7–6.2	12.0°–12.2° N	80.2°–80.3° W	1.0–3.1
21 Jul 2007	2.9–5.8	9.5°–9.9° N	84.3°–84.6° W	1.0–4.8
22 Jul 2007	11.0–12.2	12.2°–15.1° N	78.4°–79.1° W	1.0–1.6
24 Jul 2007	10.6	5.3° N	85.1°–85.4° W	1.0–1.3
22 Jul 2007	7.9–8.6	8.4°–8.6° N	84.6° W	1.4–3.6
28 Jul 2007	11.6–11.9	13.6°–14.6° N	81.8°–82.8° W	1.0–2.2
28 Jul 2007	10.4–11.9	8.7°–9.7° N	86.4°–87.3° W	1.0–2.0
29 Jul 2007	6.3–7.4	8.8°–9.2° N	84.4° W	1.0–1.5
29 Jul 2007	9.7–10.7	1.2°–7.5° N	84.3°–84.9° W	1.0–2.2
29 Jul 2007	11.0–12.1	6.5°–9.9° N	78.8°–81.8° W	1.0–2.1
3 Aug 2007	9.4–12.2	7.7°–9.3° N	80.1°–83.8° W	1.0–2.3
5 Aug 2007	11.0–11.5	6.0°–8.9° N	78.0°–82.0° W	1.0–1.3
6 Aug 2007	9.8–10.3	2.3°–6.1° N	88.8°–92.2° W	1.2–2.2
8 Aug 2007	9.4–12.2	5.8°–8.9° N	81.2°–84.2° W	1.0–2.2
10 Aug 2007	8.9–11.0	11.8°–16.3° N	85.5°–87.5° W	1.0–1.8

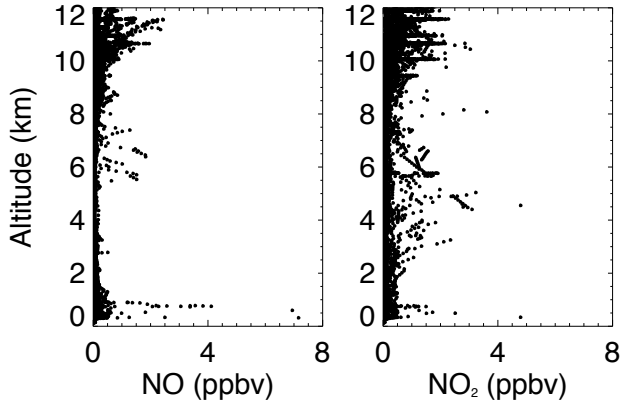

Fig. 13. NO and NO_2 measurements aboard the DC-8 aircraft during TC4. All measurements taken at least 10 min after take-off and 10 min before landing at a distance of >50 km from the airport in Alajuela, Costa Rica airport (10.0° N, 84.2° W) are shown.

enhancements of $LtNO_x$ are likely in the lower troposphere. In fact, the DC-8 data from at least two TC4 flights near active convection found NO_x enhancements in the 3.5–7.5 km altitude region (21 and 29 July 2007, see Tables 4 and 5). Given the location of our ozonesonde profile on the southern edge of the dissipating convective cell, either of these possibilities may explain our sonde observation. Furthermore, the changes observed by the ozonesonde during the 108 min of its oscillation do not represent typical variability within this layer during a single day of the TC4 mission. To assess this variability, we examine the differences between ascending and descending ozonesonde measurements from 2.5–5.1 km, measurements that are typically separated by ∼2 h in time and ∼100 km. Using all flights with both ascending and descending data within this layer taken during TC4, we find that only ∼30% of data in this altitude range showed absolute changes >4 ppbv, only ∼5% of data in this altitude range showed absolute changes of >12 ppbv; only ∼13% of all data showed differences >+4 ppbv and <1% showed changes >+12 ppbv. We also note that for the 5 August flight, 100% of the data from 2.6–5.1 km show O_3 increases. Of the 14 flights for which we have descending data at more than 50% of the levels from 2–6 km, only 3 flights (other than the 5 August flight) had at least 80% of the levels in this altitude range with increased O_3, with mean increases of 5.8 ± 3.4 ppbv, 3.7 ± 2.6 ppbv, and 2.8 ± 1.3 ppbv. These differences are less than those seen on the 5 August, which showed a mean increase of 7.8 ± 2.2 ppbv. Thus, the 5 August flight appears unique among all of our TC4 ozonesonde flights in terms of ozone changes observed over ∼2 h between 2 and 6 km.

Wind profiles from the sonde and NPOL data indicate some vertical divergence within the layer of observed O_3 changes. Subsequent trajectory calculations suggest the possible separation of the originally sampled air mass from that sampled on the final ascent by 15–30 km over the ∼108 min. Thus, horizontal O_3 gradients with a scale <30 km and/or in situ photochemistry may explain some of the sonde-observed changes in O_3. In the former case, the original air mass at 2.75 km ends up ∼15 km to the southwest of balloon

Table 5. Measurements of $NO_2 > 1$ ppbv, >50 km away from Alajuela, Costa Rica airport (10.0° N, 84.2° W) from DC-8 flights during TC4. Enhanced NO < 8 km are highlighted orange over Columbia and blue over open water.

Date	Altitude (km)	Latitudes	Longitudes	NO_2 (ppbv)
21 Jul 2007	10.4–10.7	2.5–6.3° N	76.1–77.5° W	1.0–1.3
21 Jul 2007	0.5–0.6	4.2° N	73.6° W	1.0–1.8
22 Jul 2007	0.3	8.3	84.8° W	7.2–14.2
22 Jul 2007	10.5–11.6	6.1°–7.9° N	80.7°–84.2° W	1.0–2.3
22 Jul 2007	12.2	11.3°–12.6° N	78.2°–84.2° W	1.0–1.3
24 Jul 2007	0.3	5.4° N	85.8° W	1.3–2.5
29 Jul 2007	5.5–7.4	8.8°–9.4° N	84.4° W	1.0–1.8

trajectory (see Table 3), so the balloon ends up falling backward relative to the westward moving center of the cell and the original air mass. As O_3 increases, the dynamical explanation would require higher O_3 concentrations outside of the cell in less dense clouds in which photochemical O_3 production may take place and in which loss of O_3 through reactions with NO from lightning may not have occurred. At 3.75 and 4.75 km, however, the trajectories suggest the original air mass ends up 25–30 km southeast of the balloon trajectory, resulting in the balloon sampling air closer to the center of the cell. After the last oscillation, the balloon position is on the southeastern edge of the storm, whereas for the first oscillation it was just west of the center of the cell. At these higher altitudes, it would seem that the balloon is sampling air more representative of the cell core, which suggests O_3 levels within the cell have actually increased. Thus, we argue that the changes observed by the ozonesonde cannot be explained entirely by entrainment into or detrainment from the convective cell.

Assuming the sonde-observed changes in O_3 are representative of the entire cell ($\sim$5300 km^2), an increase of $\sim 3.0 \times 10^6$ moles of O_3 between 2.5–5.1 km may be associated with this storm. Based on comparisons of the ozonesonde profile with in situ profiles from the DC-8, the total increase in O_3 from 2.5–12 km may have been (3.1–4.2) $\times 10^6$ moles, a result that suggests 70–97% of the increase occurred in the 2.5–5 km layer.

Lidar data from the DC-8 also indicated large O_3 differences between the profiles taken downwind and upwind of the cell: the lidar data report $\sim 1.3 \times 10^7$ more moles of O_3 after the passing of the cell between 1.6–8.5 km, with 6.3×10^6 of those between 2.5–5.1 km and 8.6×10^6 between 1.6–6.0 km. These differences could be due to spatial gradients in O_3, but the horizontal scale over which those gradients appear is $\sim$550 km, much greater than the $\sim$30 km horizontal distance (measured relative to the convective cell motion) over which the ozonesonde detected similarly large changes.

Furthermore, if we reduce our ozonesonde LtpcO_3 estimate by 30% to account for changes in O_3 that can be attributed to descending air with higher O_3, we find $\sim(2.1–2.5) \times 10^6$ moles of O_3 created, an estimate which agrees within a factor of two of our best estimates from the WWLLN data ($\sim 1.2 \times 10^6$ moles), from the NPOL data ($\sim 1.0 \times 10^6$ moles), and from the OMI LtNO_2 data ($\sim 1.7 \times 10^6$ moles, provided we scale by the larger area considered with the WWLLN data rather than the convective core area indicated by the NPOL data), although the estimates from the WWLLN and NPOL data carry large uncertainties due to the large uncertainties associated with the parameters included in the photochemical production calculations.

Finally, we estimate direct production of $(1.39 \pm 0.70) \times 10^6$ moles of O_3 from coronal discharges (during the two-hour period after launch) from the lightning data derived from NPOL. We note, however, that this scenario is not supported by the WWLLN data, in which little to no lightning is detected after the ozonesonde launch.

6 Conclusions

While the precise mechanism responsible for the O_3 changes observed by the oscillating ozonesonde remains uncertain, several possibilities are suggested by the data. We list them here in order, with the one we find most likely first. (1) If lightning and photochemistry are responsible for the changes in O_3, our ozonesonde observations are consistent with the hypothesis that shortly after the lightning strikes, NO reacts with O_3 forming NO_2 and leading to O_3 loss within the clouds. This hypothesis is supported by the modeling studies of Ott et al. (2007) and Salzmann et al. (2008), the thunderstorm observations in Ridley et al. (2006), and the laboratory data of Franzblau (1991). By the time the convective cell reaches the Panama coast, the lightning has subsided (as suggested by the WWLLN data in Table 2) and the clouds have begun to dissipate. Ozone within the clouds, therefore, may be relatively depleted compared to its pre-storm values, and our balloon measurements may represent measurements at various stages of recovery as NO_x photochemistry begins to favor production of O_3. (2) New O_3 may have been produced within the cloud, as suggested by Winterrath et al. (1999), who report a 62% increase in O_3 within

thunderstorm clouds, mainly attributed to non-lightning discharges; Shlanta and Moore (1972), who found O_3 levels 2.6 times higher at 6 km inside a cloud than pre-storm readings at the surface; and Clark and Griffing (1985), who reported 250% increases downwind of thunderstorms near Baltimore in 1980. If the dissipating cell was still producing lightning after launch, as suggested by the NPOL hourly flash estimates (Table 3), it is possible that direct production of O_3 from coronal discharges occurred within the cloud, as suggested by Minschwaner et al. (2008). However, the absence of detected lightning strokes in the WWLLN record as well as the rapid dissipation of the cell as it came over land argue against the importance of this mechanism in explaining the changes observed by the sonde. (3) Mixing of air lower in ozone from near the surface lofted by the convection and air higher in O_3 from above sinking near the edge of the convection may have occurred. Of course, some combination of these processes is also quite likely. Future measurements campaigns and modeling studies will be required to identify the relative importance of these processes. Nevertheless, our ozonesonde dataset provides the modeling community with new and important constraints that can be applied to future studies of O_3 production associated with tropical convective cells.

Acknowledgements. Funding for this work was provided by NASA's Upper Air Research Program (M. J. Kurylo and K. W. Jucks, program managers). Thanks to the OMI team for the total column ozone data; to Robert Holzworth for the WWLLN lightning data; to William Brune (Penn State University) for the chemical box model; to Ron Cohen, Paul Wooldridge, and Anne Perring (Univ. of California, Berkeley) for the DC-8 NO and NO_2 data; and to undergraduate students Kelsey Obenour and Danielle Slotke for helpful calculations. Special thanks to Alex Bryan and David Lutz for spending a month in the field launching our ozonesondes and to Brett Taubman (Appalatian State University) for leading the deployment of the NATIVE trailer. We also would like to thank the reviewers for their helpful comments for improving our manuscript. Finally, the authors gratefully acknowledge the NOAA Air Resources Laboratory (ARL) for the provision of the HYSPLIT transport and dispersion model and/or READY website (http://www.arl.noaa.gov/ready.php).

Edited by: T. Bertram

References

Avery, M. A., Twohy, C., McCabe, D., Joiner, J., Severance, K., Atlas, E., Blake, D., Bui, T.P., Crounse, J., Dibb, J., Diskin, G., Lawson, P., McGill, M., Rogers, D., Sachse, G., Scheuer, E., Thompson, A.M., Trepte, C., Wennberg, P., and Ziemke, J: Tropospheric ozone distribution by convection in the central American ITCZ region: Evidence from observations of ozone and clouds during the Tropical Composition, Cloud and Climate Coupling Experiment, J. Geophys. Res., 115, D00J21, doi:10.1029/2009JD013450, 2010.

Beirle, S., Salzmann, M., Lawrence, M. G., and Wagner, T.: Sensitivity of satellite observations for freshly produced lightning NO_x, Atmos. Chem. Phys., 9, 1077–1094, doi:10.5194/acp-9-1077-2009, 2009.

Bhartia, P. K.: Algorithm Theoretical Basis Document, http://toms.gsfc.nasa.gov/version8/v8toms_atbd.pdf, 2007.

Boccippio, D. J.: A diagnostic analysis of the VVP single-Doppler retrieval technique, J. Atmos. Oceanic Technol., 12, 230–248, 1995.

Bucselam, E. J., Celarier, E. A., Wenig, M. O., Gleason, J. F., Veefkind, J. P., Boersma, K. F., and Brinksma, E. J.: Algorithm for NO_2 vertical column retrieval from the Ozone Monitoring Instrument, IEEE T. Geosci. Remote, 44, 1245–1258, 2006.

Bucsela, E. J., Perring, A. E., Cohen, R. C., Boersma, K. F., Celarier, E. A., Gleason, J. F., Wenig, M. O., Bertram, T. H., Wooldridge, P. J., Dirksen, R., and Veefkind, J. P.: Comparison of tropospheric NO_2 from in situ aircraft measurements with near-real-time and standard product data from OMI, J. Geophys. Res., 113, D16S31, doi:10.1029/2007JD008838, 2008.

Bucsela, E. J, Pickering, K. E., Huntemann, T., Cohen, R. C., Perring, A. E., Gleason, J. F. Blakeslee, R., Navano, D. V., Mora Segura, I. M., Hernández, A. P., and Laporte-Molina, S.: Lightning-generated NO_x seen by OMI during NASA's TC^4 experiment, J. Geophys. Res., 115, D00J10, doi:10.1029/2009JD013118, 2010.

Celarier, E. A., Brinksma, E. J., Gleason, J. F., Veefkind, J. P., Cede, A., Herman, J. R., Ionov, D., Goutail, F., Pommeraeau, J.-P., Lambert, J.-C., van Roosendael, M., Pinardi, G., Bojkov, B., Mount, G., Spinei, E., Sander, S. P., Bucsela, E. J., Swart, D. P. J., Volten, H., Kroon, M., and Levelt, P. F.: Validation of Ozone Monitoring Instrument nitrogen dioxide columns, J. Geophys. Res., 113, D15S15, doi:10.1029/2007JD008908, 2008.

Chameides, W. L.: Effect of variable energy input on nitrogen-fixation in instantaneous linear discharges, Nature, 277 (5692), 123–125, 1979.

Chameides, W. L., Stedman, D. H., Dickerson, R. R., Rusch, D. W., and Cicerone, R. J.: NO_x production in lightning, J. Atmos. Sci., 34(1), 143–149, 1977.

Clark, J. F. and Griffing, G. W.: Aircraft observations of extreme ozone concentrations near thunderstorms, Atmos. Environ., 19, (7), 1175–1179, 1985.

Cooper, O. R., Stohl, A., Trainer, M., Thompson, A.M., Witte, J.C., Oltmans, S. J., Morris, G., Pickering, K. E., Crawford, J. H., Chen, G., Cohen, R. C., Bertram, T.H., Wooldridge, P., Perring, A., Brune, W.H., Merrill, J., Moody, J. L., Tarasick, D., Nedelec, P., Forbes, G., Newchurch, M. J., Schmidlin, F. J., Johnson, B. J., Turquety, S., Baughcum, S. L., Ren, X., Fehsenfeld, F.C., Meagher, J. F., Spichtinger, N., Brown, C. C., McKeen, S. A., McDermid, I. S., and Leblanc, T. : Large upper tropospheric ozone enhancements above mid-latitude North America during summer: In situ evidence from the IONS and MOZAIC ozone networks, J. Geophys. Res., 111, D24S05, doi:10.1029/2006JD007306, 2006.

Cooper, O. R., Trainer, M., Thompson, A. M., Oltmans, S. J., Tarasick, D. W., Witte, J. C., Stohl, A., Eckhardt, S., Lelieveld, J., Newchurch, M. J., Johnson, B. J., Portmann, R. W., Kalnajs, L., Dubey, M. K., Leblanc, T., McDermid, I. S., Forbes, G., Wolfe, D., Carey-Smith, T., Morris, G. A., Lefer, B., Rappenglueck,

B., Joseph, E., Schmidlin, F., Meagher, J., Fehsenfeld, F. C., Keating, T. J., Van Curen, R. A., and Minschwaner, K.: Evidence for a recurring eastern North America upper tropospheric ozone maximum during summer, J. Geophys. Res., 112, D23304, doi:10.1029/2007JD008710, 2007.

Cummins, K. L., Murphy, M. J., Bardo, E. A., Hiscox, W. L., Pyle, R. B., and Pifer, A. E.: A combined TOA/MDF technology upgrade of the U.S. Lightning Detection Network, J. Geophys. Res., 103, D8, 9035–9044, 1998.

DeCaria, A. J., Pickering, K. E., Stenchikov, G. L., and Ott, L. E.: Lightning-generated NO_x and its impact on tropospheric ozone production: A three-dimensional modeling study of a Stratospher-Troposphere Experiment: Radiation, Aerosols and Ozone (STERAO-A) thunderstorm, J. Geophys. Res., 110(D14), D14303, doi:10.1029/2004JD005556, 2005.

Dickerson, R. R., Huffman, G. J., Luke, W. T., Nunnermacker, L. J., Pickering, K. E., Leslie, A. C. D., Lindsey, C. G., Slinn, W. G. N., Kelly, T. J., Daum, P. H., Delany, A. C., Greenberg, J. P., Zimmerman, P. R., Boatman, J. F., Ray, J. D., and Stedman, D. H.: Thunderstorms: An important mechanism in the transport of air pollutants, Science, 235, 460–465, 1987.

Doherty, R. M., Stevenson, D. S., Collins, W. J., and Sanderson, M. G.: Influence of convective transport on tropospheric ozone and its precursors in a chemistry-climate model, Atmos. Chem. Phys., 5, 3205–3218, doi:10.5194/acp-5-3205-2005, 2005.

Drapcho, D. L., Sisterson, D., and Kumar, R.: Nitrogen fixation by lightning activity in a thunderstorm, Atmos. Environ., 17, 729–734, 1983.

Draxler, R. R. and Rolph, G.D.: HYSPLIT (HYbrid Single-Particle Lagrangian Integrated Trajectory) Model access via NOAA ARL READY Website (http://ready.arl.noaa.gov/HYSPLIT.php), NOAA Air Resources Laboratory, Silver Spring, MD, 2010.

Duncan, B. N., Strahan, S. E., Yoshida, Y., Steenrod, S. D., and Livesey, N.: Model study of the cross-tropopause transport of biomass burning pollution, Atmos. Chem. Phys., 7, 3713–3736, doi:10.5194/acp-7-3713-2007, 2007.

Fehr, T., Holler, H., and Huntrieser, H.: Model study on production and transport of lightning-produced NO_x in a EULINOX supercell storm, J. Geophys. Res., 109(D9), D09102, doi:10.1029/2003JD003935, 2004.

Fontijn, A., Sabadell, A. J., and Ronco, R. J.: Homogenous chemiluminescent measurement ofnitric oxide with ozone, Anal. Chem., 42, 575–579, 1970.

Franzblau, E.: Electrical discharges involving the formation of NO, NO_2, HNO_3, and O_3, J. Geophys. Res., 96, D12, 22,337–22,345, 1991.

Futyan, J. M. and Del Genio, A. D.: Relationships between lightning and properties of convective cloud clusters, Geophys. Res. Lett. 34, L15705, doi:10.1029/2007GL030227, 2007.

Grant, W. B., Pierce, R. B., Oltmans, S. J., and Browell, E. V.: Seasonal evolution of total and gravity wave induced laminae in ozonesonde data in the tropics and subtropics, Geophys. Res. Lett., 25, 1863–1866, 1998.

Grewe, V.: The impact of climate variability on tropospheric ozone, Sci. Total Environ., 374, 167–181, 2007.

Griffing, G. W.: Ozone and oxides of nitrogen production during thunderstorms, J. Geophys. Res., 82, 943–950, 1977.

Hudman, R. C., Jacob, D. J., Turquety, S., Leibensperger, E. M., Murray, L.T., Wu, S., Gilliland, A. B., Avery, M., Betram, T. H., Brune, W., Cohen, R. C., Dibb, J. E., Flocke, F. M., Fried, A., Holloway, J., Newuman, J. A., Orville, R., Perring, A., Ren, X., Sachse, G. W., Singh, H. B., Swanson, A., and Wooldridge, P. J.: Surface and lightning sources of nitrogen oxides over the United States: Magnitudes, chemical evolution, and outflow, J. Geophys. Res., 112, D12S05, doi:10.1029/2006JD007912, 2007.

Huntrieser, H., Schumann, U., Schlager, H., Höller, H., Giez, A., Betz, H.-D., Brunner, D., Forster, C., Pinto Jr., O., and Calheiros, R.: Lightning activity in Brazilian thunderstorms during TROCCINOX: implications for NO_x production, Atmos. Chem. Phys., 8, 921–953, doi:10.5194/acp-8-921-2008, 2008.

Jenkin, M. E., Saunders, S. M., and Pilling, M. J.: The tropospheric degradation of volatile organic compounds: a protocol for mechanism development, Atmos. Environ., 31, 81–104, 1997.

Jenkins, G. S., Camara, M., and Ndiaye, S. A.: Observational evidence of enhanced middle/upper tropospheric ozone via convective processes over the equatorial tropical Atlantic during the summer of 2006, Geophys. Res. Lett., 35, L12806, doi:10.1029/2008GL033954, 2008.

Koike, M., Kondo, Y., Kita, K., Takegawa, N., Nishi, N., Kashihara, T., Kawakami, S., Kudoh, S., Blake, D., Shirai, T., Liley, B., Ko, M., Miyazaki, Y., Kawaski, Z., and Ogawa, T.: Measurements of reactive nitrogen produced by tropical thunderstorms during BIBLE-C, J. Geophys. Res., 112, D18304, doi:10.1029/2006JD008193, 2007.

Komhyr, W. D.: Operations Handbook: Ozone measurements to 40 km altitude with mode 4A electrochemical concentration cell (ECC) ozonesondes (used with 1680-Mhz radiosondes), NOAA Technical Memorandum ERLARL-149, 1986.

Komhyr, W. D., Barnes, R. A., Brothers, G. B., Lathrop, J. A., and Opperman, D. P.: Electrochemical concentration cell performance evaluation during STOIC, J. Geophys. Res., 100, 9231–9244, 1995.

Kroening, J. and Ney, E.: Atmospheric Ozone, J. Geophys. Res., 67(5), 1867–1875, 1962.

Lawrence, M. G., Chameides, W. L., Kasibhatla, P. S., Levy, II, H. and Moxim, W.: Lightning and atmospheric chemistry: the rate of atmospheric NO production, 189–202, in: Handbook of Atmospheric Electrodynamics, Vol. I, edited by: Volland, H., CRC Press, Inc., Boca Raton, USA, 1995.

Lawrence, M. G., von Kuhlmann, R., Salzmann, M., and Rasch, P. J.: The balance of effects of deep convective mixing on tropospheric ozone, Geophys. Res. Lett., 30, 1940, doi:10.1029/2003GL017644, 2003.

Lay, E. H., Rodger, C. J., Holzworth, R. H, Jacobson, A. R., Suszcynsky, D. M., Thomas, J. N., and Brundell, J. B.: World-wide lightning location network: improvements in global detection efficiency and estimated stroke energy, Fourth Conference on the Meteorological Applications of Lightning Data, American Meteorological Society, Phoenix, AZ, 2009.

Levelt, P. F., Hilsenrath, E., Leppelmeier, G. W., van den Oord, G. B. J., Bhartia, P. K., Tamminen, J., de Haan, J. F., and Veefkind, J. P.: Science objectives of the Ozone Monitoring Instrument, IEEE Trans Geo. Rem. Sens., 44(5), 1199–1208, 2006.

Levelt, P. F., van den Oord, G. B. J., Dobber, M. R., Malkki, A., Visser, H., deVries, J., Stammes, P., Lundell, J. O. V., and Saari, H.: The Ozone Monitoring Instrument, IEEE Trans Geo. Rem. Sens., 44(5), 1093–1101, 2006.

Lelieveld, J. and Crutzen, P. J.: Role of deep cloud convection in the ozone budget of the troposphere, Science, 264, 1759–1761, 1994.

Levine, J. S., Rogowski, R. S., Gregory, G. L., Howell, W. E., and Fishman, J.: Simultaneous measurements of NO_x, NO, and O3 production in a laboratory discharge: Atmospheric implications, Geophys. Res. Lett., 8, 4, 357–360, 1981.

Lin, X., Trainer, M., and Liu, S.C.: On the nonlinearity of tropospheric ozone production, J. Geophys. Res., 93, 15,879–15,888, 1988.

Martin, R. V., Sauvage, B., Folkins, I., Sioris, C. E., Boone, C., Bernath, P., and Ziemke, J.: Space-based constraints on the production of nitric oxide by lightning, J. Geophys. Res., 112, D09309, doi:10.1029/2006JD007831, 2007.

McGill, M. J., Li, L., Hart, W. D., Heymsfield, G. M., Hlavka, D. L., Racette, P. E., Tian, L., Vaughan, M. A., and Winker, D. M.: Combined lidar-radar remote sensing: Initial results from CRYSTAL-FACE, J. Geophys. Res., 109, D07203, doi:10.1029/2003JD004030, 2004.

McPeters, R. D., Labow, G. J., and Johnson, B. J.: A satellite-derived ozone climatology for balloonsonde estimation of total column ozone, J. Geophys. Res., 102(D7), 8875–8886, 1997.

McPeters, R., Kroon, M., Labow, G., Brinksma, E., Balis, D., Petropavlovskikh, I., Veefkind, J. P., Bhartia, P. K., and Levelt, P. F.: Validation of the Aura Ozone Monitoring Instrument total column ozone product, J. Geophys. Res., 113, D15S14, doi:10.1029/2007JD008802, 2008.

Minschwaner, K., Kalnajs, L. E., Dubey, M. K., Avallone, L. M., Sawaengphokai, P. C., Edens, H. E., and Winn, W. P.: Observation of enhanced ozone in an electrically active storm over Socorro, NM: Implications for ozone production from corona discharges, J. Geophys. Res., 113, D17208, doi:10.1029/2007JD009500, 2008.

Morris, G. A.: Explaining an oscillating weather balloon with a thermodynamic model, Am. J. Phys., to be submitted, 2011.

Noxon, J. F.: Atmospheric nitrogen fixation by lightning, Geophys. Res. Lett., 3, 8, 463–465, 1976.

Orville, R. E.: Ozone production during thunderstorms, measured by the absorption of ultraviolet radiation from lightning, J. Geophys. Res., 72, 14, 3557–3561, 1967.

Ott, L. E., Pickering, K. E., Stenchikov, G. L., Huntrieser, H., and Schumann, U.: Effects of lightning NO_x production during the 21 July European Lightning Nitrogen Oxides Project storm studied with a three-dimensional cloud-scale chemical transport model, J. Geophys. Res., 112, D05307, doi:10.1029/2006JD007365, 2007.

Ott, L., Pickering, K. E., Stenchikov, G., Allen, D., DeCaria, A., Ridley, B., Lin, R.-F., Lang, S., and Tao, W.-K.: Production of lightning NO_x and its vertical distribution calculated from three-dimensional cloud-scale chemical transport model simulations, J. Geophys. Res., 115, D04301, doi:10.1029/2009JD011880, 2010.

Pearson, R. W. and Stedman, D. H.: Instrumentation for fast response ozone measurements from aircraft, Atmos. Tech., 12, 51–55, 1980.

Peyrous, R. and Lapeyre, R.-M.: Gaseous products created by electrical discharges in the atmosphere and condensation nuclei resulting from gaseous phase reactions, Atmos. Environ., 16, 5, 959–968, 1982.

Pfister, G. G., Emmons, L. K., Hess, P. G., Lamarque, J.-F., Thompson, A. M., Yorks, J. E.: Analysis of the Summer 2004 Ozone Budget over North America using IONS Observations and MOZART-4 Simulations, J. Geophys. Res., 113, D23306, doi:10.1029/2008JD010190, 2008.

Pickering, K. E., Thompson, A. M., Dickerson, R. R., Luke, W. T., McNamara, D. P., Greenberg, J. P., and Zimmerman, P. R.: Model calculations of tropospheric ozone production potential following observed convective events, J. Geophys. Res., 95, 14,049–14,062, 1990.

Pickering, K. E., Thompson, A. M., Wang, Y., Tao, W.-K., McNamara, D. P., Kirchhoff, V. W. J. H., Heikes, B. G., Sachse, G. W., Bradshaw, J. D., Gregory, G. L., and Blake, D. R.: Convective transport of biomass burning emissions over Brazil during TRACE-A, J. Geophys. Res., 101, 23,993–24,012, 1996.

Pickering, K. E., Wang, Y., Tao, W.-K., Price, C., and Müller, J.-F.: Vertical distributions of lightning NO_x for use in regiona and global chemical transport models, J. Geophys. Res., 103(D23), 31,203–31,216, 1998.

Pickering, K. E., Huntrieser, H., and Schumann, U.: Chapter 26: Lightning and NO_x production in global models in Lightning: Principles, Instruments and Applications, edited by: Schumann, U., and Laroche, P., doi:10.1007/978-1-4020-9079-0-26, 2009.

Pierce, E. T.: Latitudinal variation of lightning parameters, J. Appl. Meteor., 9, 194–195, 1970.

Prentice, S. A. and Mackerras, D.: The ratio of cloud to cloud-ground lightning flashes in thunderstorms, J. Appl. Meteor., 16, 545–549, 1977.

Price, C. and Rind, D.: A simple lightning parameterization for calculating global lightning distributions, J. Geophys. Res., 97(D9), 9919–9933, 1992.

Price, C., Penner, J., and Prather, M.: NO_x from lightning 1: Global distribution based on lightning physics, J. Geophys. Res., 102(D5), 5929–5941, 1997.

Ridley, B., Ott, L., Pickering, K., Emmons, L., Montzka, D., Weinheimer, A., Knapp, D., Grahek, F., Li, L., Heymsfield, G., McGill, M., Kucera, P., Mahoney, M.J., Baumgardner, D., Schultz, M., and Brasseur, G.: Florida thunderstorms: A faucet of reactive nitrogen to the upper troposphere, J. Geophys. Res., 109, D17305, doi:10.1029/2004JD004769, 2004.

Ridley, B. A., Avery, M. A., Plant, J. V., Vay, S. A., Montzka, D. D., Weinheimer, A. J., Knapp, D. J., Dye, J. E., and Richard, E. C.: Sampling of chemical constituents in electrically active convective systems: Results and cautions, J. Atmos. Chem., 54, 1–20, doi:10.1007/s10874-005-9007-5, 2006.

Rodger, C. J., Werner, S., Brundell, J. B., Lay, E. H., Thomson, N. R., Holzworth, R. H., and Dowden, R. L.: Detection efficiency of the VLF World-Wide Lightning Location Network (WWLLN): initial case study, Ann. Geophys., 24, 3197–3214, 2006.

Salzmann, M., Lawrence, M. G., Phillips, V. T. J., and Donner, L. J.: Cloud system resolving model study of the roles of deep convection for photo-chemistry in the TOGA COARE/CEPEX region, Atmos. Chem. Phys., 8, 2741–2757, doi:10.5194/acp-8-2741-2008, 2008.

Sander, S. P., Friedl, R. R., Ravishankara, A. R., Golden, D. M., Kolb, C. E., Kurylo, M. J., Molina, M. J., Moortgat, G. K., Keller-Rudek, H. J., Finlayson-Pitts, B., Wine, P. H., Huie, R. E., and Orkin, V. L.: Chemical Kinetics and Photochemical Data for Use in Atmospheric Studies, Evaluation Number 15, JPL Publication 06-2, NASA Jet Propulsion Laboratory, Pasadena,

California, 2006.

Schlanta, A. and Moore, C.B.: Ozone and point discharge measurements in thunderclouds, J. Geophys. Res., 77, 24, 4500–4510, 1972.

Schoeberl, M. R. and Sparling, L.: Trajectory modeling, in Diagnostic Tools in Atmospheric Physics, Proceedings of the International School of Physics "Enrico Fermi", 124, edited by: Fiocco, G. and Visconti,G., 289–306, IOS Press, Washington DC, 1995.

Schoeberl, M. R., Douglass, A. R., Hilsenrath, E., Bhartia, P. K., Beer, R., Waters, J. W. Gunson, M. R., Froidevaux, L., Gille, J. C., Barnett, J. J., Levelt, P. E., and DeCola, P.: Overview of the EOS Aura Mission, IEEE T. Geosci. Remote, 44(5), 1066–1074, 2006.

Schumann, U. and Huntrieser, H.: The global lightning-induced nitrogen oxides source, Atmos. Chem. Phys., 7, 3823–3907, doi:10.5194/acp-7-3823-2007, 2007.

Shon, Z.-H., Madronich, S., Song, S.-K., Flocke, F. M., Knapp, D. J., Anderson, R. S., Shetter, R. E., Cantrell, C. A., Hall, S. R., and Tie, X.: Characteristics of the NO-NO2-O_3 system in different chemical regimes during the MIRAGE-Mex field campaign, Atmos. Chem. Phys., 8, 7153–7164, doi:10.5194/acp-8-7153-2008, 2008.

Skamarock, W. C., Dye, J. E., Defer, E., Barth, M. C., Stith, J. L., Ridley, B. A., and Baumann, K.: Observational- and modeling-based budget of lightning produced NO_x in a continental thunderstorm, J. Geophys. Res., 108(D10), 4305, doi:10.1029/2002JD002163, 2003.

Smit, H.G., Straeter, W., Johnson, B. J., Oltmans, S. J., Davis, J., Tarasick, D. W., Hoegger, B., Stubi, R., Schmidlin, F. J., Northam, T., Thompson, A. M., Witte, J. C., Boyd, I., and Posny, F.: Assessment of the performance of ECC-ozonesondes under quasi-flight conditions in the environmental simulation chamber: Insights from the Jülich Ozone Sonde Intercomparison Experiment (JOSIE), J. Geophys. Res., 112, D19306, doi:10.1029/2006JD007308, 2007.

Stockwell, W. R., Kirchner, F., Kuhn, M., and Seefeld, S.: A new mechanism for regional atmospheric chemistry modeling, J. Geophys. Res., 102, 25,847–825,879, 1997.

Theisen, C. J., Kucera, P. A., and Poellot, M. R.: A study of relationships between tropical thunderstorm properties and corresponding anvil cloud characteristics, J. Meteor. and Climate, 48(9), 1882–1901, 2009.

Thompson, A. M., Tao, W.-K., Pickering, K. E., Scala, J. R., and Simpson, J.: Tropical deep convection and ozone formation, Bull. Amer. Met. Soc., 78, 1,043–1,054, 1997.

Thompson, A. M., Witte, J. C., McPeters, R. D., Oltmans, S. J., Schmidlin, F. J., Logan, J. A., Fujiwara, M., Kirchhoff, V. W. J. H., Posny, F., Coetzee, G. J. R., Hoegger, B., Kawakami, S., Ogawa, T., Johnson, B. J., Vömel, H., and Labow, G.: Southern Hemisphere Additional Ozonesondes (SHADOZ) 1998–2000 tropical ozone climatology 1. Comparison with Total Ozone Mapping Spectrometer (TOMS) and ground-based measurements, J. Geophys. Res., 108(D2), 8238, doi:10.1029/2001JD000967, 2003.

Thompson, A. M., Stone, J. B., Witte, J. C., Miller, S. K., Pierce, R. B., Chatfield, R. B., Oltmans, S. J., Cooper, O. R., Loucks, A. L., Taubman, B. F., Johnson, B. J., Joseph, E., Kucsera, T. L., Merrill, J. T., Morris, G. A., Hersey, S., Forbes, G., Newchurch, M. J., Schmidlin, F.J., Tarasick, D.W., Thouret, V., and Cammas, J.-P.: IONS (INTEX Ozonesonde Network Study, 2004), 1. Summertime UT/LS (Upper Troposphere/Lower Stratosphere) ozone over northeastern North America, J. Geophys. Res., 112, D12S12, doi:10.1029/2006JD007441, 2007a.

Thompson, A. M., Stone, J. B., Witte, J. C., Miller, S. K., Oltmans, S. J., Kucsera, T. L., Ross, K. L., Pickering, K. E., Merrill, J. T., Forbes, G., Tarasick, D. W., Joseph, E., Schmidlin, F. J., McMillan, W. W., Warner, J., Hintsa, E. J., and Johnson, J. E: Intercontinental Transport Experiment Ozonesonde Network Study (IONS, 2004): 2. Tropospheric Ozone Budgets and Variability over Northeastern North America, J. Geophys. Res., 112, D12S13, doi:10.1029/2006JD007670, 2007b.

Thompson, A. M., Witte, J. C., Smit, H. G. J., Oltmans, S. J., Johnson, J. J., Kirchhoff, V. W. J. H., and Schmidlin, F. J.: Southern Hemisphere Additional Ozonesondes (SHADOZ) 1998–2004 tropical ozone climatology. 3. Instrumentation, Station Variability, Evaluation with Simulated Flight Profiles, J. Geophys. Res., 112, D03304, doi:10.1029/ 2005JD007042, 2007c.

Thompson, A. M., Yorks, J. E., Miller, S. K., Witte, J. C., Dougherty, K. M., Morris, G. A., Baumgardner, D., Ladino, L., and Rappenglück, B.: Tropospheric ozone sources and wave activity over Mexico City and Houston during MILAGRO/Intercontinental Transport Experiment (INTEX-B) Ozonesonde Network Study, 2006 (IONS-06), Atmos. Chem. Phys., 8, 5113–5125, doi:10.5194/acp-8-5113-2008, 2008.

Thompson, A. M., MacFarlane, A. M., Morris, G. A., Yorks, J. E., Miller, S. K., Taubman, B. F., Verver, G., Vomel, H., Avery, M. A., Hair, J. W., Diskin, G. S., Browell, E. V., Canossa, J. V., Kucsera, T. L., Klich, C. A., and Hlavka, D. L.: Convective and wave signatures in ozone profiles over the equatorial Americas: Views from TC^4 (2007) and SHADOZ, J. Geophys. Res., 115, D00J23, doi:10.1029/2009JD012909, 2010.

Thornton, J. A., Wooldridge, P. J., and Cohen, R. C.: Atmospheric NO_2: In situ laser-induced fluorescence detection at parts per trillion mixing ratios, Anal. Chem., 72, 528–539, 2000.

Toon, O. B., Starr, D. O., Jensen, E. J., Newman, P. A., Platnick, S., Schoeberl, M. R., Wennberg, P. O., Wofsy, S. C., Kurylo, M. J., Maring, H., Jucks, K. W., Craig, M. S., Vasques, M. F., Pfister, L., Rosenlof, K. H., Selkirk, H. B., Colarco, P. R., Kawa, S. R., Mace, G. G., Minnis, P., and Pickering, K. E.: Tropical Composition, Clouds, and Climate Coupling (TC4) Overview, J. Geophys. Res., 115, D00J04, doi:10.1029/2009JD013073, 2010.

Wenig, M. O., Cede, A. M., Bucsela, E. J. Celarier, E. A., Boersma, K. F., Veefkind, J. P., Brinksma, E. J., Gleason, J. F., and Herman, J. R.: Validation of OMI tropospheric NO_2 column densities using direct-sun mode Brewer measurements at NASA Goddard Space Flight Center, J. Geophys. Res., 113, D16S45, doi:10.1029/2007JD008988, 2008.

Winterrath, T., Kurosu, T. P., Richter, A., and Burrows, J. P.: Enhanced O_3 and NO_2 in thunderstorm clouds: Convection or production, Geophys. Res. Lett., 26, 9, 1291–1294, 1999.

Wood, E. C., Herndon, S. C., Onasch, T. B., Kroll, J. H., Canagaratna, M. R., Kolb, C. E., Worsnop, D. R., Neuman, J. A., Seila, R., Zavala, M., and Knighton, W. B.: A case study of ozone production, nitrogen oxides, and the radical budget in Mexico City, Atmos. Chem. Phys., 9, 2499–2516, doi:10.5194/acp-9-2499-2009, 2009.

Zaveri, R. A., Berkowitz, C. M., Kleinman, L. I., Springston, S. R., Doskey, P. V., Lonneman, W. A., and Spicer, C. W.: Ozone

production efficiency and NO_x depletion in an urban plume: Interpretation of field observations and implications for evaluating O_3-NO_x-VOC sensitivity, J. Geophys. Res., 108(D19), doi:10.1029/2002JD003144, 2003.

Zhang, R., Tie, X., and Bond, D. W.: Impacts of anthropogenic and natural NO_x sources over the U.S. on tropospheric chemistry, Proc. Natl. Acad. Sci. U. S. A., 100, 1505–1509, doi:10.1073/pnas.252763799, 2003.